Aircraft observed diurnal variations of the planetary boundary layer under heat waves 1 Yuanjie Zhang^{1,2}, Liang Wang², Joseph A. Santanello Jr.³, Zaitao Pan^{4,1}, Zhiqiu Gao¹, Dan 2 Li^{2*} 3 ¹School of Atmospheric Physics, Nanjing University of Information Science and Technology, 4 Nanjing, China 5 6 ²Department of Earth and Environment, Boston University, Boston, MA, USA ³Hydrological Sciences Laboratory, NASA Goddard Space Flight Center, Greenbelt, Maryland 7 ⁴Department of Earth and Atmospheric Sciences, Saint Louis University, St. Louis, MO, USA 8 9 * Corresponding author: Dan Li (lidan@bu.edu) 10 11 Keywords: Planetary boundary layer, heat wave, AMDAR, WVSS, atmospheric circulation 12 13

Abstract

14

15

16

17

18

19

20

21

22

23

24

25

26

27

28

29

30

31

32

33

34

35

36

This study investigates the diurnal variations of the planetary boundary layer (PBL) properties during heat waves (HWs) based on a decade-long data record of hourly profiles from the Aircraft Meteorological Data Reports (AMDAR) at 54 major airports over the Continental United States. The results are also corroborated by surface observations from weather stations. HWs are defined as periods of at least two consecutive days with daily mean temperature higher than the 95th percentile of the warm season (May to September) climatology. Temperature differences between HW and non-HW periods show strong vertical variations throughout the PBL. Under HWs, the daytime convective PBL is deeper while the nocturnal residual layer is excessively hotter. The difference between HWs and non-HWs in the PBL wind and humidity are not uniform, with clear diurnal and vertical variations at some sites. HW-related changes in PBL wind components are strongly associated with changes in atmospheric circulation patterns, especially in the northeastern region. The specific humidity in the PBL shows increases in humid regions but decreases in arid regions under HWs. Moisture transport and surface evaporation are found to play an important role in modulating the changes in PBL humidity. This study highlights that HW-related changes in the PBL structure are not uniform and are affected by both synoptic and local factors.

1. Introduction

Heat waves (HWs) pose significant threats to the human society and natural ecosystems across the globe (Perkins, 2015). Studies reported that HWs have already become unusually frequent and severe in recent years (e.g., Meehl and Tebaldi, 2004; Peterson et al., 2013), and are projected to continue to increase in duration, intensity and frequency in the future under increased greenhouse gas concentrations (e.g., Lau and Nath, 2012, 2014; Meehl et al., 2007).

One of the major concerns about HWs is their impacts on human health (Anderson and Bell, 37 2009; Anderson and Bell, 2011; Perkins, 2015; Zuo et al., 2015), especially in urban areas (e.g., 38 Li and Bou-zeid, 2013; Li et al., 2015, 2016; Ramamurthy et al., 2017; Liao et al., 2018; Ao et 39 al., 2019). Mass mortality was caused by the 2003 Europe heat wave (Coumou and Rahmstorf, 40 2012) and Russian heat wave (McMichael and Lindgren, 2011). Thus, accurate and reliable 41 predictions of such extreme events are necessary for early warning systems. However, 42 operational forecasts still fail to capture the onset and evolution of HWs since our understanding 43 of HWs is limited and their representation in climate models remains imperfect (Vautard et al., 44 45 2013; Weisheimer and Palmer, 2014). 46 In the last few decades, many studies have focused on the driving physical mechanisms of HWs (Perkins, 2015). It is now well understood that HWs are generally associated with quasi-47 stationary high-pressure systems that produce subsidence, clear skies, warm air advection, and 48 49 prolonged hot conditions near the surface (Black et al., 2004; Meehl and Tebaldi, 2004; Xoplaki et al., 2003). Meanwhile, land-atmosphere feedbacks under these synoptic conditions, including 50 the depletion of soil moisture and subsequent reduction in evaporative cooling, may further 51 amplify HWs (Alexander, 2011; Black et al., 2004; Fischer et al., 2007a; 2007b; Miralles et al., 52 2012; Miralles et al., 2014, 2018; Teuling et al., 2010). Studies revealed that soil moisture-53 54 temperature interactions play an important role in modulating the intensity (Durre et al., 2000), frequency (Fischer et al., 2007a), and persistence (Lorenz et al., 2010) of HWs. While these 55 previous studies have significantly improved our understanding of the synoptic-scale circulation 56 57 patterns (Li et al., 2019; Cassou et al., 2005; Meehl and Tebaldi, 2004; Nasrallah et al., 2004) 58 and land-atmosphere feedback mechanisms associated with and contributing to HWs, the state

and evolution of the planetary boundary layer (PBL), which is the key connecting the land surface with the synoptic systems aloft, during HWs received much less attention.

A few key exceptions include the pioneering study by Miralles et al. (2014), which revealed that in addition to the warm air advection and increasingly desiccated land surface, the enhanced entrainment of warm air into the PBL during daytime and the formation of a deep and warm nocturnal residual layer overnight, which stores heat from one day to the next, also intensifies warming during mega-heatwave events. A recent review study (Miralles et al., 2018) suggested that the land surface conditions and plant physiology at ecosystem scales can influence the dynamics of PBL during HWs, which will further affect the entrainment of warm air from the top and warm air advection. The identified key role of PBL dynamics and the lack of systematic investigations of PBL structures under HWs, especially using observational data, strongly motivate our study.

While HWs are inevitably associated with high air temperatures, it is also crucial to examine changes in the other meteorological factors, especially atmospheric humidity and wind, which are critical controls of human thermal comfort and heat stress (Barnett et al., 2010; Epstein and Moran, 2006; Matzarakis and Nastos, 2011; Zhang et al., 2014a). Atmospheric humidity and wind in the PBL can also strongly affect and be strongly affected by land surface fluxes and local circulations, thereby modulating land-atmosphere feedbacks (Karl and Knight, 1997; Santanello et al., 2018; Seneviratne et al., 2010). Few studies investigated the change of wind during HWs, although it is directly related to heat and moisture transport. HWs resulting from quasi-stationary anticyclones are often believed to be associated with low wind speed (Ackerman and Knox, 2006). However, HWs could strengthen secondary circulations (e.g., between cities and their surrounding rural areas or between land and sea) and thus possibly enhance the local wind speed

(Lebassi et al., 2009; Lebassi et al., 2011; Li et al., 2016; Li and Bou-Zeid, 2013). A recent study compared observed near-surface wind speeds under HW and non-HW conditions and found that HW-related changes in the near-surface wind speed were not uniform, with some sites showing increases and some showing decreases (Sun et al., 2017). These conflicting notions and results further motivate us to examine HW-related changes in the wind components throughout the lower troposphere and across a large number of sites/regions.

The objectives of this paper are to (1) examine the differences in near-surface and PBL air temperature, wind, and humidity between HW and non-HW conditions, (2) compare HW-related changes in the PBL structure across different climatic regions, and (3) investigate the connection between HW-related changes in PBL structures, the large-scale circulation pattern and the land-atmosphere feedback.

2. Data and methods

2.1 Hourly PBL profiles

Traditional techniques such as radiosondes cannot fully characterize the diurnal variation of the PBL due to the limited temporal resolution (typically only available at 00 and 12 UTC). On the other hand, high-resolution lidar and sodar measurements are often only available for a short period. In this study, we employ a newly developed, decade-long (from 2007 to 2016) data record of hourly PBL profiles (Zhang et al., 2019) near 54 major US airports (see Figure 1 and Table 1). This data record is based on the aircraft meteorological reports from commercial aircraft through the Aircraft Meteorological Data Relay (AMDAR) program, established by the World Meteorological Organization. The AMDAR program has grown rapidly over the past few years with about 5000 aircraft worldwide contributing more than 600,000 temperature and wind observations per day, 450,000 of which are over CONUS (Petersen, 2016). In addition, water

vapor (humidity) measurements can also be derived from the aircraft platform through a single laser-diode sensor, namely the Water Vapor Sensing System 2nd Generation (WVSS-II), which is deployed operationally by 148 aircrafts from South West Airlines and United Parcel Service principally over CONUS. The humidity data are much less compared to temperature/wind data but still cover many parts of CONUS (Petersen et al., 2016). The AMDAR data are publicly available on the Meteorological Assimilation Data Ingest System web service portal (https://madis-data.cprk.ncep.noaa.gov/madisPublic1/data/archive/). In this study, the AMDAR points failed in the **MADIS** quality control data (https://madis.ncep.noaa.gov/madis acarsp qc.shtml) are removed.

105

106

107

108

109

110

111

112

113

114

Table 1. Geographic information of the selected airports, numbers of AMDAR hourly profiles of temperature, wind and humidity in summer, and the proportion of HW days relative to total summer days from 2007 to 2016 at each airport.

	IATA	Airport name	Latitude	Longitude	Number of hourly profiles		Proportion of HW days				
	Code		(°N)	(°E)					(%	6)	
					Temperature	Wind	Humidity	90^{th}	95^{th}	98^{th}	99 th
1	ABQ	Albuquerque International Sunport	35.05	-106.62	7784	7781	1703	13.7	7.3	1.7	0.8
2	BDL	Bradley International Airport	41.93	-72.68	8472	7754	2171	13.7	6.1	2.6	1.2
3	BFI	Boeing Field	47.53	-122.30	4052	4020	412	14.6	7.0	2.6	1.2
4	BNA	Nashville International Airport	36.13	-86.68	10034	9667	2915	12.8	6.4	2.8	1.7
5	BOS	Boston Logan International Airport	42.36	-71.01	13770	13584	1840	13.3	5.8	2.0	1.1
6	BSM	Austin-Bergstrom International	30.20	-97.68	8229	8184	1647	14.5	7.0	2.2	1.0
		Airport									
7	BWI	Baltimore/Washington International	39.18	-76.67	13091	12875	4694	14.0	7.1	2.3	0.8
		Thurgood Marshall Airport									
8	CLE	Cleveland Hopkins International	41.41	-81.86	8887	5673	5258	13.3	5.5	2.2	1.2
		Airport									
9	DCA	Ronald Reagan Washington	38.85	-77.03	11971	11047	3088	13.6	6.5	2.3	1.2
		National Airport									
10	DEN	Denver International Airport	39.87	-104.67	11838	11820	3431	13.0	5.5	1.8	1.0
11	DFW	Dallas/Fort Worth International	32.90	-97.03	16180	16174	610	15.4	7.7	2.7	1.2
		Airport									
12	DTW	Detroit Metropolitan Wayne County	42.23	-83.33	10977	8301	6279	12.9	5.8	2.3	0.9
		Airport									
13	EWR	Newark Liberty International	40.70	-74.17	11551	10916	1689	13.8	7.0	2.1	0.9
		Airport									
14	FLL	Fort Lauderdale-Hollywood	26.07	-80.15	9891	9845	1379	12.9	6.2	2.4	1.1
		International Airport									
15	GEG	Spokane International Airport	47.63	-117.53	6060	4516	2360	14.6	7.3	2.6	1.4
16	HOU	William P. Hobby Airport	29.65	-95.28	10747	10747	3230	14.6	7.6	2.5	1.5

			• • • • •		0046	-0					
17	IAD	Dulles International Airport	38.98	-77.47	8836	7965	3120	13.8	6.1	2.7	1.3
18	IAH	George Bush Intercontinental	29.97	-95.35	7203	5336	2050	15.2	6.6	2.5	1.0
		Airport									
19	IND	Indianapolis International Airport	39.73	-86.27	10490	9033	2872	13.3	6.3	2.8	1.1
20	JFK	John F. Kennedy International	40.65	-73.78	12748	12283	1876	13.7	6.4	2.2	1.1
		Airport									
21	LAS	McCarran International Airport	36.08	-115.17	14256	14226	4133	14.0	7.0	2.8	1.4
22	LAX	Los Angeles International Airport	33.93	-118.40	17648	17606	4268	15.0	7.5	3.0	1.3
23	LGA	LaGuardia Airport	40.77	-73.87	12842	11875	5207	14.7	6.3	1.6	1.0
24	MCI	Kansas City International Airport	39.32	-94.72	9811	9687	2400	14.6	6.7	2.4	0.9
25	MCO	Orlando International Airport	28.43	-81.32	12948	12879	2866	13.0	6.5	2.6	1.2
26	MDW	Chicago Midway International	41.78	-87.75	10767	10766	3752	13.0	5.5	2.1	1.2
		Airport									
27	MEM	Memphis International Airport	35.05	-90.00	13271	11924	3292	14.9	6.3	2.4	1.7
28	MHT	Manchester-Boston Regional	42.93	-71.43	4282	3981	940	12.6	6.6	2.5	1.4
		Airport									
29	MIA	Miami International Airport	25.82	-80.28	16994	16988	1351	12.1	5.5	2.2	0.4
30	MSP	Minneapolis-Saint Paul	44.88	-93.22	12308	9887	6359	13.8	5.9	2.4	1.2
		International Airport									
31	MSY	Louis Armstrong New Orleans	29.98	-90.25	8152	7843	1790	13.4	6.5	2.2	1.1
		International Airport									
32	OAK	Oakland International Airport	37.73	-122.22	13224	13161	3014	12.6	6.5	1.6	0.9
33	OKC	Will Rogers World Airport	35.40	-97.60	5686	5290	1296	15.1	7.6	2.3	1.2
34	OMA	Eppley Airfield	41.30	-95.90	5355	4982	1243	12.9	5.9	2.4	1.4
35	ONT	Ontario International Airport	34.05	-117.62	10949	10929	1698	14.2	7.2	2.1	1.3
36	ORD	O'Hare International Airport	41.98	-87.90	15447	15333	719	13.2	5.8	2.3	1.1
37	PDX	Portland International Airport	45.60	-122.60	12292	11078	3765	14.0	6.4	2.2	1.2
38	PHL	Philadelphia International Airport	39.87	-75.24	13543	12585	5039	13.7	6.8	2.4	1.2
39	PHX	Phoenix Sky Harbor International	33.43	-112.02	13088	13075	3782	14.2	6.7	2.2	0.9
		Airport									
40	PIT	Pittsburgh International Airport	40.50	-80.23	6097	5318	1569	13.3	6.2	2.2	0.7
41	RDU	Raleigh-Durham International	35.87	-78.78	9400	8434	2443	14.5	7.2	2.6	1.5
		Airport									
42	RNO	Reno-Tahoe International Airport	39.50	-119.78	6833	6089	2134	13.8	6.6	2.6	1.3
43	SAN	San Diego International Airport	32.73	-117.17	11598	11597	2492	14.2	7.7	2.7	1.2
44	SAT	San Antonio International Airport	29.53	-98.47	7763	7717	1767	14.7	5.7	2.3	0.7
45	SDF	Louisville International Airport	38.18	-85.73	13872	12820	6385	12.9	6.6	2.3	1.1
46	SEA	Seattle-Tacoma International	47.45	-122.30	15715	14716	5650	13.5	6.7	2.3	0.9
		Airport									
47	SFO	San Francisco International Airport	37.62	-122.38	12403	12397	1405	12.9	6.2	2.3	0.9
48	SJC	Norman Y. Mineta San Jose	37.37	-121.92	9882	9607	2723	13.2	5.3	2.5	0.9
		International Airport									
49	SLC	Salt Lake City International Airport	40.77	-111.97	6910	6906	1226	13.0	6.6	2.0	1.4
50	SMF	Sacramento International Airport	38.70	-121.60	9282	9005	2587	13.0	5.7	2.0	0.8
51	SNA	John Wayne Airport	33.67	-117.88	10040	10040	1055	15.4	7.3	2.8	1.4
52	STL	St. Louis Lambert International	38.74	-90.36	12300	11723	4056	14.2	6.3	2.5	1.5
		Airport									
53	TPA	Tampa International Airport	27.97	-82.53	10375	10334	2062	14.0	6.5	1.7	0.7
54	TUL	Tulsa International Airport	36.20	-95.90	6412	6193	974	14.5	6.6	2.8	1.5



Figure 1. Location of the selected airports over CONUS. Airports chosen for case studies are highlighted in red.

As the raw AMDAR data are irregular in space and time and include ascent/descent phases near airports and the cruise phase, we developed a new data record by merging all ascent and descent soundings within one hour and by interpolating them onto a vertical grid in terms of regular and linear heights (Zhang et al., 2019). Note that here each hourly grid time (e.g., 1 pm) represents an hourly interval (1-2 pm) after the grid time. In our previous study (Zhang et al., 2019), we used 20 m as the vertical resolution for interpolation (i.e., we would have 75 data points below 1500 m). This relatively high resolution is affordable because we merge all ascent and descent soundings within one hour, hence the vertical resolution of the new data record is enhanced compared to a single ascent or descent sounding. We note that the actual number of measurements in the lower atmosphere within an hour varies across time and space, with some

airports having on average over 100 data points below 1500 m. We also note that the interpolation can be done at other resolutions (e.g., 50 m or 100 m) and in terms of pressure levels (e.g., every 20 hPa) depending on the application and data availability. Here we choose 20 m because of our focus on the lower atmosphere (from 0 to 3000 m, including the PBL). The total numbers of hourly PBL profiles of temperature, wind and humidity in summer are shown in Table 1. By interpolating the AMDAR data onto radiosonde levels, Zhang et al. (2019) also compared the new data record to the nearby radiosonde data and found good agreement between the two datasets for air temperature, specific humidity, and wind components. It is worth mentioning that while previous studies often reported warm biases associated with AMDAR data (Ballish and Kumar, 2008), Zhang et al. (2019) found that such warm biases were typically large at high altitudes but insignificant at low altitudes. Figure 2 shows an example of hourly AMDAR PBL temperature profiles at McCarran International Airport (LAS, see Table 1) in 2013 during which a HW occurred from DOY 179 to 185 (the identification of HW event will be discussed in Section 2.4). Although there are missing data (typically occurring from the mid-night to early morning due to the lack of air traffic), especially for specific humidity, the diurnal variations are reasonably well captured.

132

133

134

135

136

137

138

139

140

141

142

143

144

145

146

147

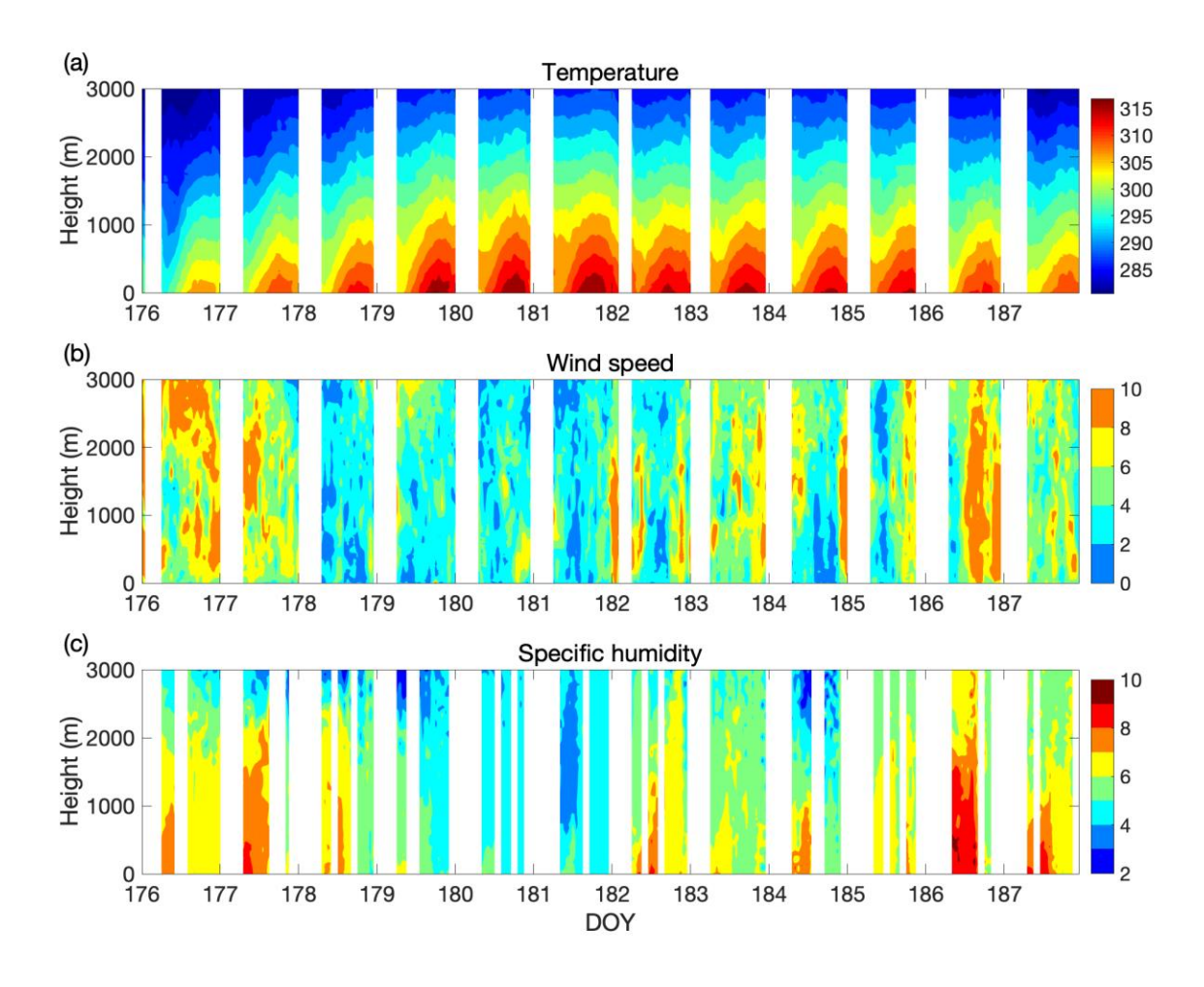


Figure 2. Temporal evolution of temperature, wind speed, specific humidity profiles derived from AMDAR data from 25 June to 6 July, 2013 at LAS (see Table 1 for the airport's full name). The blank areas indicate hours that have no data.

2.2 Surface observations

To characterize the surface climatic conditions, we use weather station observations from the Integrated Surface Database (ISD) provided by National Oceanic and Atmospheric Administration (NOAA, https://www.ncdc.noaa.gov/isd/data-access). These data within or near the selected 54 airports are hourly averaged to match the AMDAR PBL profiles. A qualitative comparison between surface observations ISD and the lowest 5 points (from 20 to 100 m) of

AMDAR profiles will be conducted to examine the reliability of AMDAR data for studying the diurnal variation of the PBL.

2.3 Reanalysis data

To investigate the synoptic-scale atmospheric circulation patterns and land-atmosphere feedbacks associated with HWs, the North America Regional Reanalysis (NARR), which has a spatial resolution of 32 km and 29 pressure levels, is used. First, the temperature, wind and specific humidity data from NARR are compared with those from AMDAR in terms of summer averaged profiles (Figure S1-S2) and HW signatures (Figure S3). The results show good agreement between the two datasets, suggesting that it is reasonable to use the geopotential height field and surface latent heat flux from NARR to illustrate the synoptic-scale atmospheric circulation patterns and land-atmosphere feedbacks associated with HWs.

2.4 HW definition

There is no unified definition for HWs (Meehl and Tebaldi, 2004). Commonly used HW definitions in the literature vary in terms of the temperature metrics employed (maximum, mean, minimum), the thresholds for "extreme", the length of consecutive days, and the period of the reference climate (Smith et al., 2013). HW indices are divided into two major groups according to the type of threshold used: relative thresholds (De Boeck et al., 2010; Meehl and Tebaldi, 2004) and absolute thresholds (Frich et al., 2002; Robinson, 2001). There are locational variations in the absolute threshold in defining HWs and using an absolute threshold does not take into account climatic variability (De Boeck et al., 2010). Radinović and Ćurić (2012) suggested using relative thresholds derived from the normal frequency distribution of daily temperature values rather than absolute thresholds, since HW definition should permit a comparison of results across climatic zones.

In this study, a HW are defined as a period in which the daily mean temperature of at least 2 consecutive days exceeds the 95th percentile of the warm season (1 May through 30 September) climatology defined based on the period 2007-2016 (Anderson and Bell, 2011). The daily mean temperature is taken from the surface observations. We note that different thresholds (90th, 95th, 98th, and 99th percentiles) have been used in previous studies for defining HWs (Smith et al., 2013). The proportions of HW days for different thresholds are shown in Table 1. The moderate threshold (95th percentile) is chosen as a compromise between ensuring that differences between HW periods and non-HW periods are significant to be detected and maintaining a reasonably large sample of HW events.

3. Results

The results are presented in terms of diurnal variations of PBL temperature, wind components, and humidity profiles averaged over HW and non-HW (typical summer) days during the period from 2007 to 2016. Hours in which the total number of profiles over the period of 2007-2016 is less than 10 for temperature and wind and 5 for humidity are shown as blank areas (again typically from mid-night to early morning). A less stringent requirement is used for humidity due to the relatively small amount of AMDAR humidity samples. In this study, we do not focus on the onset and development of individual HWs. Instead, the overall features of diurnal temperature, wind and humidity profiles over HW and non-HW conditions are investigated. The findings generated from AMDAR data are corroborated by the surface observations from weather stations (i.e., from ISD).

Four airports, including the Louisville International Airport (SDF), Philadelphia International Airport (PHL), William P. Hobby Airport at Houston (HOU), and Denver International Airport (DEN) are chosen for case studies (see Figure 1 for their locations). They are chosen mainly

based on the availability of humidity observations since many airports have too few humidity data to construct a complete diurnal cycle. In addition, these four airports cover different climate regimes over CONUS. Results from the other airports will be also shown.

It is expected that the PBL profiles are strongly affected by the synoptic-scale atmospheric circulation patterns and land-atmosphere feedbacks, which will be also examined in this study to better understand changes in PBL wind and humidity during HW periods. In the meantime, it should be noted that most of the airports are near or in major cities. As a result, local factors, such as urban land use, might also play a role in modifying the PBL profiles, although it is difficult to separate such local effects from the synoptic controls.

3.1 Comparisons between AMDAR data and surface observations

To corroborate the findings from AMDAR data, surface observations and the lower part (20-100 m) of AMDAR profiles are first compared in Figure 3. It can be also seen that the AMDAR temperature averaged over 20-100 m (triangles) is lower than the average surface air temperature during daytime, while slightly higher than or equal to the average surface air temperature at night (Figure 3a-d). This is consistent with the expectation that the surface is typically warmer than the air during daytime but cooler during nighttime. The AMDAR wind components averaged within 20-100 m are smaller than the surface observations for zonal wind at PHL and meridional wind at SDF and HOU (Figure 3e-l). This might be caused by two factors. First, more frequent aircraft maneuvers in the lower layer can cause large errors in the airspeed vector determination (Bisiaux et al., 1983). Second, there are stronger turbulent fluctuations and larger small-scale wind variations in the surface layer (Benjamin et al., 1999). However, the sign of the differences between HW and non-HW periods and the diurnal trends are basically the same for the lower part (20-100 m) of AMDAR profiles and surface data, which suggests that the AMDAR data

should still capture the wind differences between HW and non-HW periods. For humidity, the lower part (20-100 m) of AMDAR data agree reasonably well with the surface observations (Figure 3m-p), confirming the reliability of the AMDAR humidity data for examining the diurnal climatology.



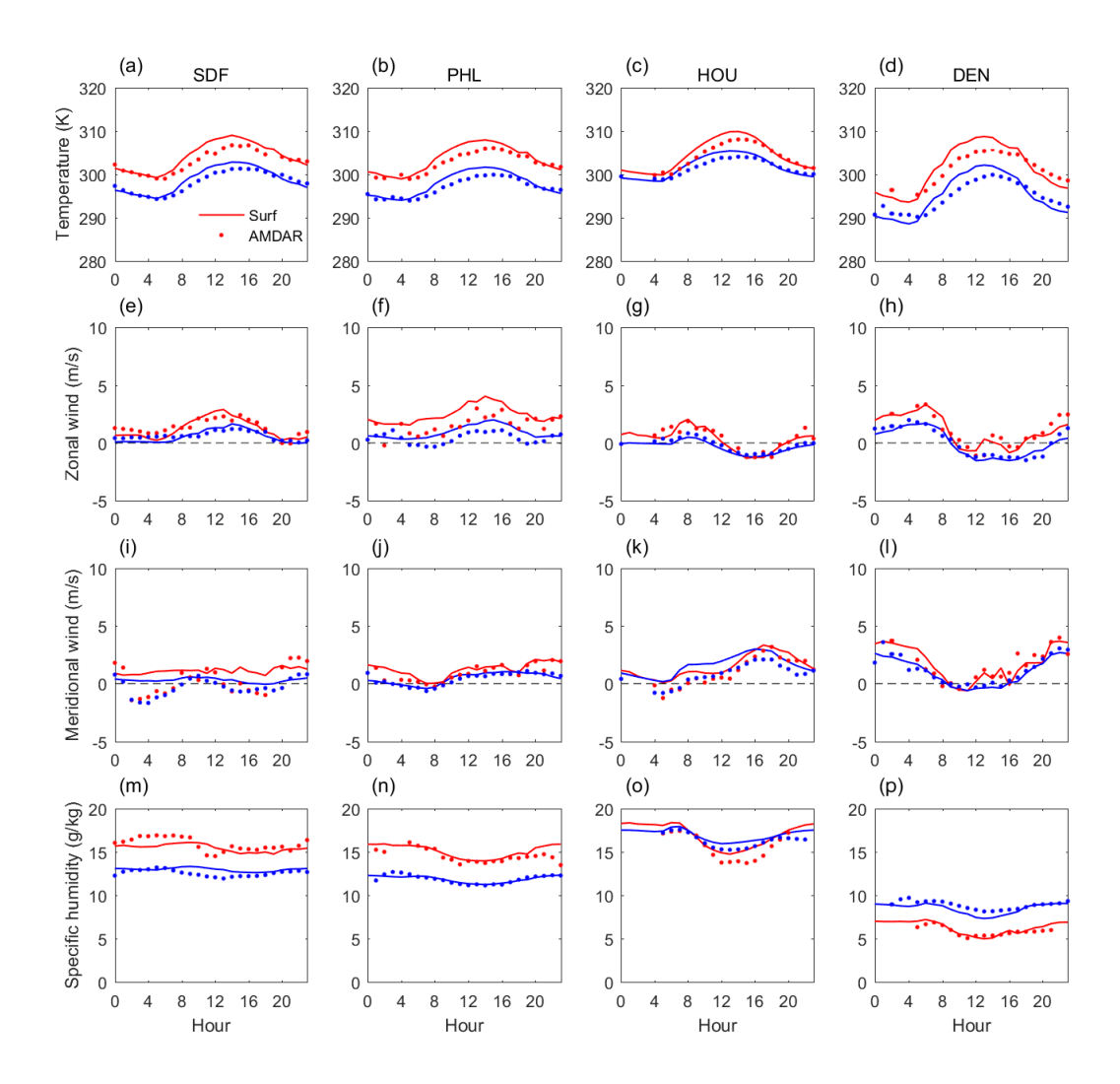


Figure 3. Comparisons of (a-d) air temperature, (e-h) zonal wind, (i-l) meridional wind, and (m-p) specific humidity between the low part (20-100 m) of AMDAR profiles and surface observations averaged from 2007 to 2016 at SDF, PHL, HOU and DEN. Red and blue indicate HW and non-HW periods, respectively.

3.2 HW-related changes in the PBL structure

3.2.1 Temperature

240

241

242

243

244

245

246

247

248

249

250

251

252

253

254

255

256

257

Figures 4-5 present the vertical and diurnal variations of temperature averaged over HW and non-HW periods and their differences at SDF, PHL, HOU, and DEN. Note that local standard time is used throughout the paper. During both HW and non-HW periods, the PBL temperature shows strong diurnal variations at the four airports, with the maximum temperature around 14:00, and the diurnal variations weaken with height. Compared to non-HW periods, HW periods are associated with much higher surface air temperature (Figure 3a-d) and PBL temperature (Figures 4 and 5). The PBL temperature shows the formulation of "heat domes" under HWs, indicating that HWs are associated with temperature increases not only at the surface but also throughout the PBL. In terms of surface air temperature, the differences between HW and non-HW periods have no clear diurnal variation at these airports (Figure 3a-d), except for HOU where the surface air temperature difference reaches its maximum around 14:00 and minimum at night (this can be inferred from Figure 3c). Similar to surface air temperature, there is no obvious diurnal variation in the PBL temperature differences between HW and non-HW periods at SDF, PHL and DEN, while the PBL temperature differences at HOU show a maximum in the afternoon (Figure 4e-f and 5e-f).

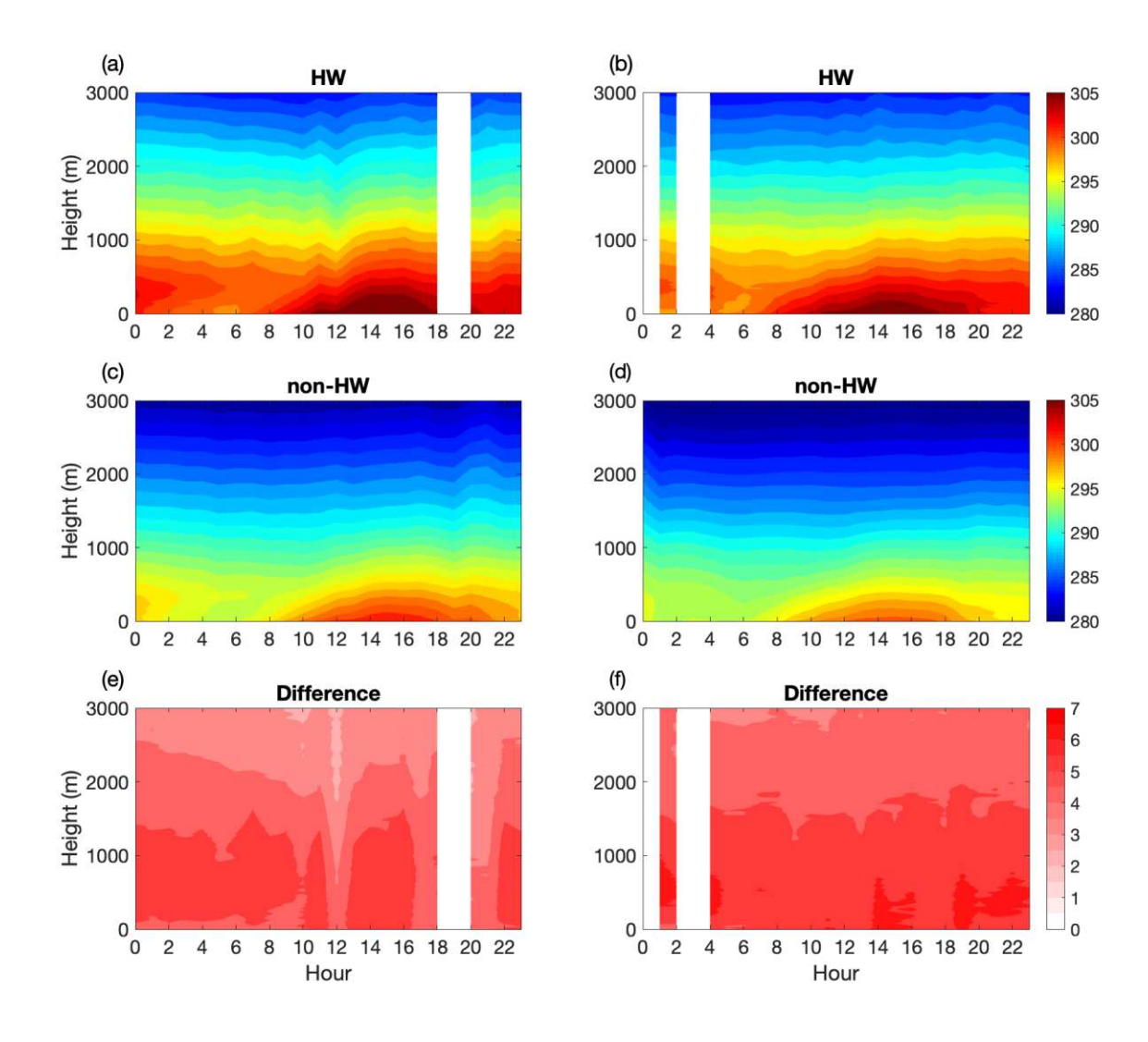


Figure 4. Diurnal variations of temperature during (a-b) HW and (c-d) non-HW periods in the lowest 3000 m above the ground averaged from 2007 to 2016, and (e-f) HW-related changes. The left column shows results at SDF and the right column shows results at PHL. Units are K.

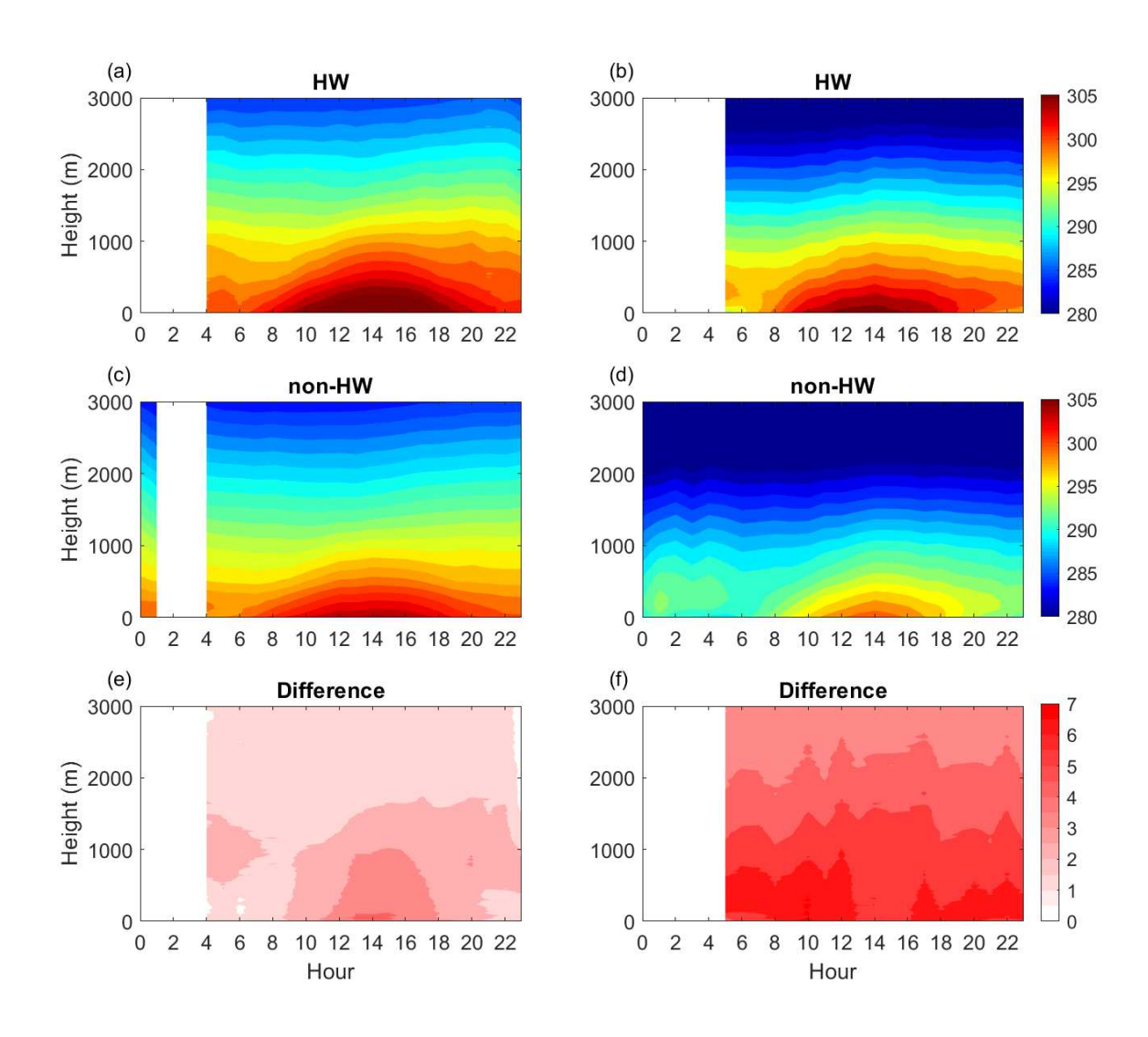


Figure 5. Similar to Figure 4, but at HOU (left) and DEN (right).

The strong temporal and vertical variations of the PBL temperature highlight the advantage and the unique value of the AMDAR data. In particular, certain features identified by the AMDAR profiles are impossible with the conventional twice daily soundings or surface observations. For example, the diurnal variation of the temperature difference between HW and non-HW conditions at HOU can be only identified with the AMDAR profiles.

To further investigate the effect of HWs on the PBL height, Figure 6 shows the vertical profiles of potential temperature (θ) during HW and non-HW periods and their differences at the four airports. The PBL heights under HW and non-HW periods are shown as the dashed and solid lines, respectively. Here the PBL height is estimated by the bulk Richardson number method (Vogelezang and Holtslag, 1996) with a critical value of 0.25 (Hong, 2010; Zhang et al., 2014b). The bulk Richardson number method is chosen to compute the PBL height since it considers both potential temperature and wind profiles, and in theory should work under all atmospheric stratification conditions. It can be seen that the daytime PBL height is strongly increased under HWs but the nighttime PBL height is not. At nighttime (04:00, local standard time), the strongest HW-related potential temperature increase is located near the PBL top at SDF, PHL, and DEN and above the PBL top at HOU. This vertical pattern of HW-related potential temperature increase, with weaker warming near the surface but stronger warming near or above the PBL top, plays an important role in enhancing the thermal inversion at night, which might explain why the nighttime PBL height is not strongly increased (and even slightly decreased for PHL and HOU) under HWs. On the other hand, the strong HW-related warming above the PBL contributes to the formulation of deep and warm nocturnal residual layers, especially at DEN (Figure 6d), which serves as a positive feedback to intensify the following day's PBL potential temperature by releasing the heat into the PBL through entrainment (Miralles et al., 2014). At daytime (14:00, local standard time), a convective PBL is observed and the strongest HWrelated warming occurs within the PBL, which intensifies dry convection and raises the height of

270

271

272

273

274

275

276

277

278

279

280

281

282

283

284

285

286

287

288

289

290

291

the convective PBL. This can lead to entrainment of warm air from the previously mentioned

nocturnal residual layer and upper layers, which further contributes to the escalation of PBL potential temperature (Miralles et al., 2014).

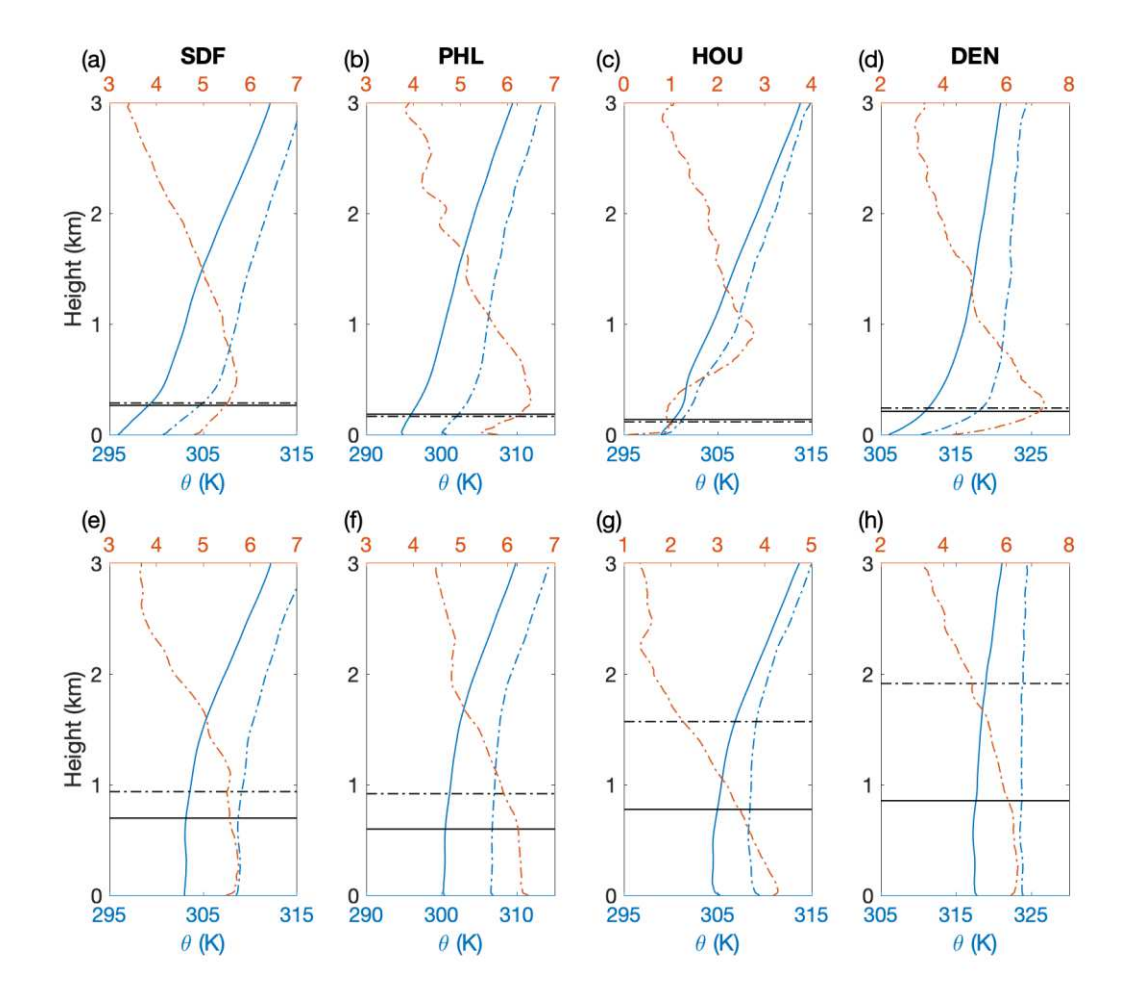


Figure 6. Vertical profiles of potential temperature (θ) during HW (blue dashed curves) and non-HW periods (blue solid curves) at 04:00 (upper panels) and 14:00 (bottom panels) at four airports SDF, PHL, HOU, and DEN. Also shown are their differences (red dashed curves). Dashed and solid horizontal lines indicate the diagnosed PBL heights for HW and non-HW periods, respectively.

3.2.2 Wind components

304

305

306

307

308

309

310

311

312

313

314

315

316

317

318

319

320

321

322

323

324

325

326

Figure 7 shows the diurnal variations of zonal and meridional wind averaged over HW and non-HW periods and their differences at PHL. The results indicate prevailing westerly (Figure 7a) and southerly (Figure 7b) winds in the PBL but northerly winds above the PBL up to 3000 m (Figure 7b). Compared to non-HW periods, the vertical and diurnal variations of the wind components show similar patterns during HW periods. The HW-related differences in the zonal wind are positive at almost all levels below 3000 m throughout the day, with maxima in the PBL during the nighttime (Figure 7e). However, the HW-related differences in the meridional wind show vertical and diurnal variations. Overall, the southerly wind in the PBL and the northerly wind above the PBL (up to 3000 m) are both enhanced under HW periods. Given that the zonal wind (westerly) is increased and the meridional wind is also enhanced (both in and above the PBL), this suggests that the wind speed in the low troposphere (below 3000 m) is increased under HWs. The strong vertical variation in the HW-related changes in the meridional wind further implies that the traditional analysis of HW-related wind changes at or near the surface cannot represent the characteristics of wind changes in the whole PBL. The results at HOU are shown in Figure 8. During typical summer conditions, the zonal wind changes from westerly to easterly around 12:00 below 2000 m and remains easterly above 2000 m, while the meridional wind generally shows as southerly wind throughout the day (Figure 8cd). The HW-related changes of the zonal wind are positive below 1000 m but negative above, which generally strengthen the lower westerly wind and upper easterly wind. Both the lower increases and the upper decreases are stronger at night (Figure 8e). The HW-related changes of the meridional wind are generally negative, implying a decrease in the southerly wind or even a switch to northerly wind (see the upper layer in Figure 8b). However, the HW-related changes of the meridional wind are positive below 500 m between 16:00 and 24:00 (Figure 8f), which seem to exhibit the feature of low-level jets. These findings demonstrate strong diurnal variations associated with HW-related changes in PBL wind components.

The results above indicate that HW-related changes in PBL wind components vary vertically and diurnally at a given airport and vary among airports. As mentioned in the introduction, HW events are generally caused by quasi-stationary high pressure systems (Meehl and Tebaldi, 2004; Perkins, 2015), which is expected to cause low wind speed. On the other hand, since most airports are located in or near cities and some are located in coastal areas, changes in PBL wind components may be also associated with the strengthened secondary circulations over urbanrural and/or land-sea gradients during HW periods (Hidalgo et al., 2010; Lebassi et al., 2011; Li et al., 2016; Li and Bou-Zeid, 2013; Ohashi and Kida, 2002). Thus, the large variability associated with HW-related changes in PBL wind components might be the outcome of a combination of changes in synoptic-scale atmospheric circulation patterns, which will be further

discussed in Section 3.3, and changes in local- to regional-scale circulations.

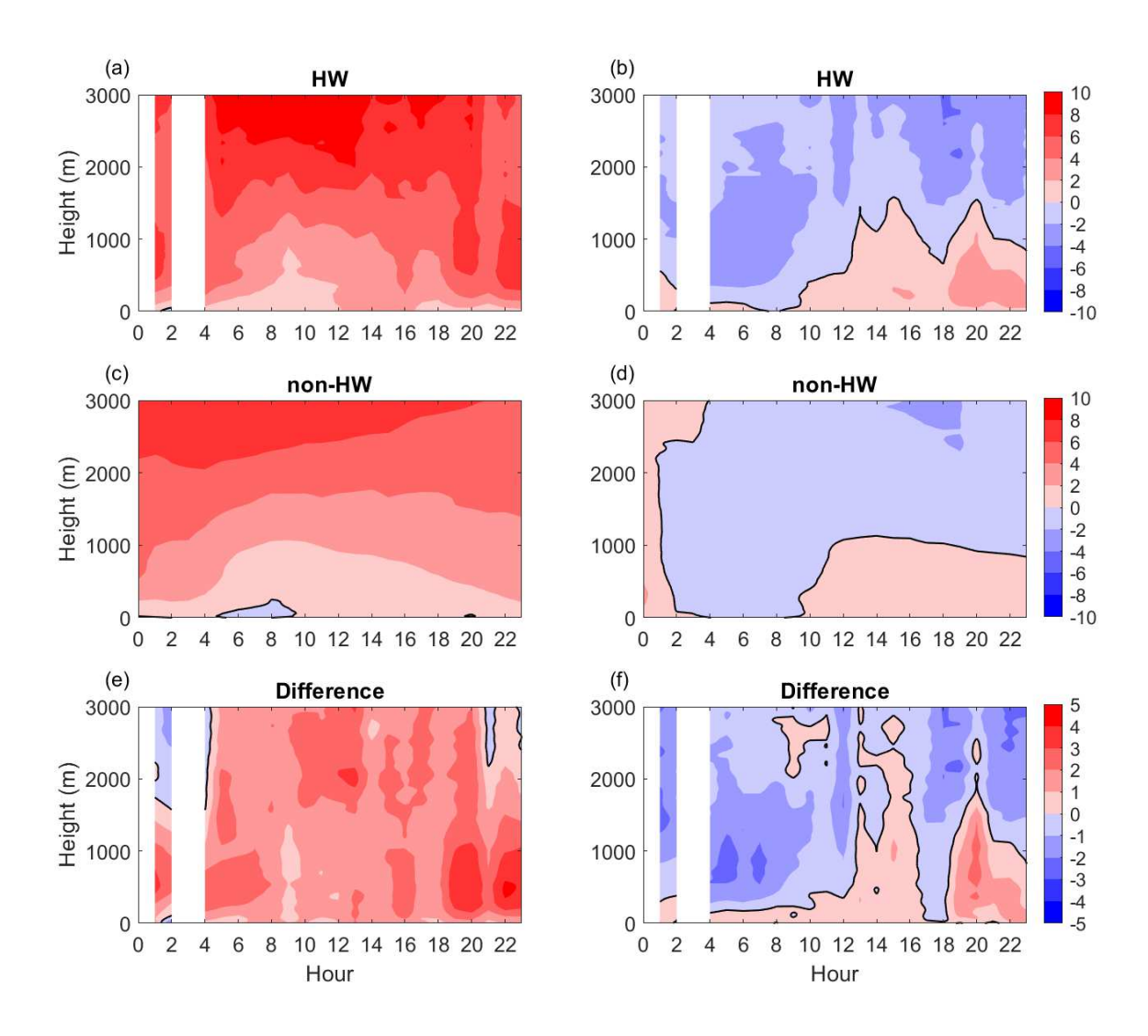


Figure 7. Diurnal variations of zonal (left) and meridional wind (right) during (a-b) HW and (c-d) non-HW periods in the lowest 3000 m above the ground averaged from 2007 to 2016, and (e-f) HW-related changes at PHL. Black lines indicate zero values. Units are m/s.

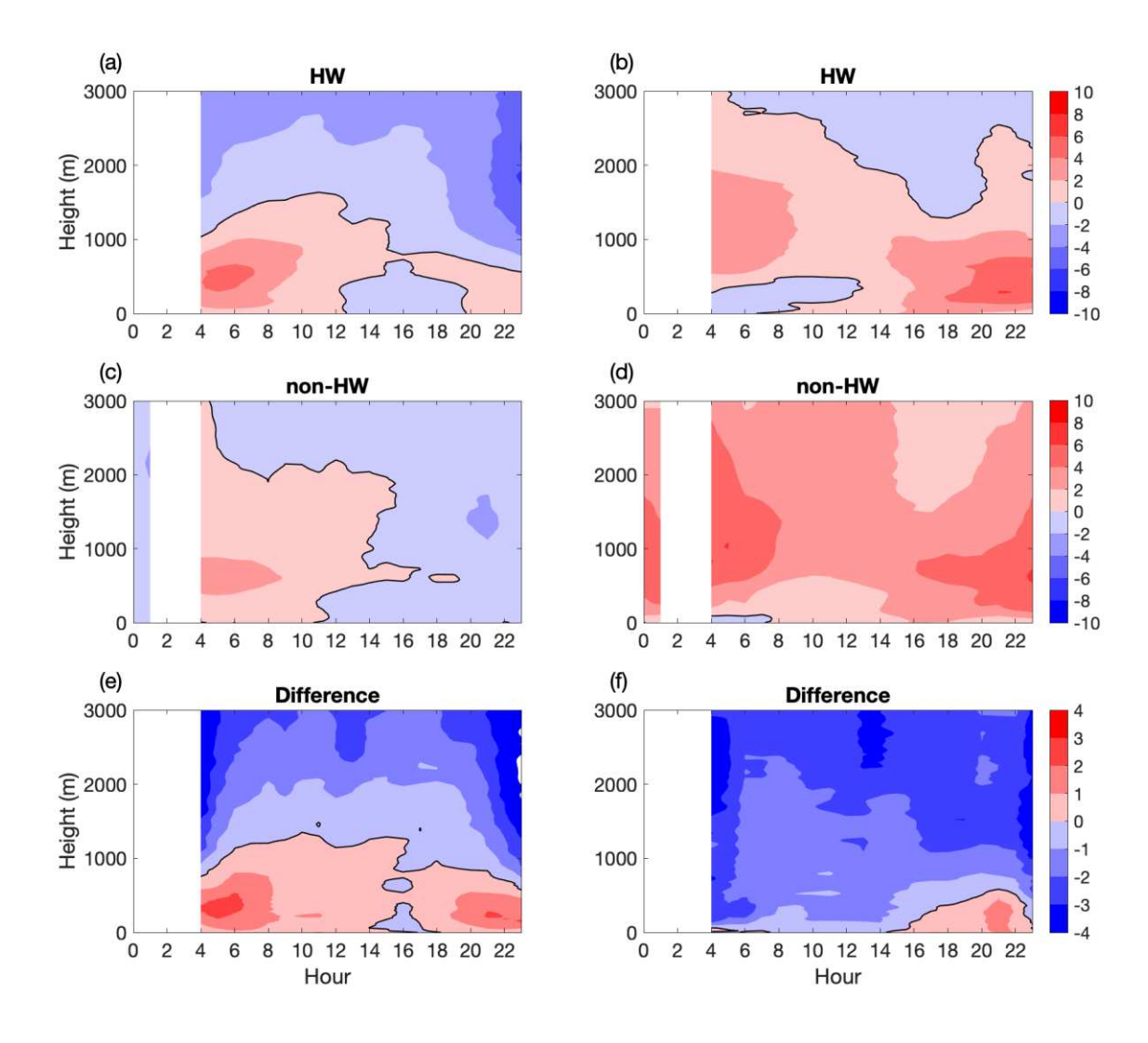


Figure 8. Similar to Figure 7, but at HOU.

3.2.3 Humidity

The diurnal variations of specific humidity averaged over HW and non-HW periods and their differences at SDF, PHL, HOU, and DEN are shown in Figures 9 and 10. There are clear diurnal variations in the specific humidity near the surface at SDF and PHL during both HW and non-HW periods. The specific humidity in the PBL is generally higher at night and lower during the daytime, showing a bi-modal pattern with two maxima at early morning and late evening,

respectively (Figure 9a-d). The HW-related changes in specific humidity are generally positive below 3000 m throughout the day at SDF and PHL. The humidity change is relatively large in the PBL and decreases with height (Figure 9e-f). Given that the airports SDF and PHL are located in humid zones according to the regional categorization in Findell and Eltahir (2003), the increase of humidity during HW periods is likely caused by the increased surface evapotranspiration. Under HWs, a high atmospheric demand for water vapor caused by the higher air temperature incentivizes soil evaporation and plant water consumption through transpiration (Liu et al., 2015; Teuling et al., 2013). For moist soils, there is enough moisture in the soil to meet the high atmospheric demand during HW and thus the specific humidity in the PBL is increased. In addition to surface evapotranspiration, changes in the humidity at SDF and PHL may also be affected by changes in wind conditions (see Figure 7 for PHL and Figures 11 and 12). As the PBL height increases, especially for convective PBLs, dry air entrainment will reduce the PBL specific humidity (Santanello et al., 2007), which will to some extent offset the increase of specific humidity caused by surface evapotranspiration. As shown in Figure 6, the increase of PBL height during HWs relative to non-HWs is negligible for stable PBLs (e.g., in the early morning), so the reduction of specific humidity due to the PBL growth and dry air entrainment is

354

355

356

357

358

359

360

361

362

363

364

365

366

367

368

369

370

371

372

morning hours as shown in Figure 9e-f.

small. This may explain why the maximum increase of specific humidity generally occurs in the

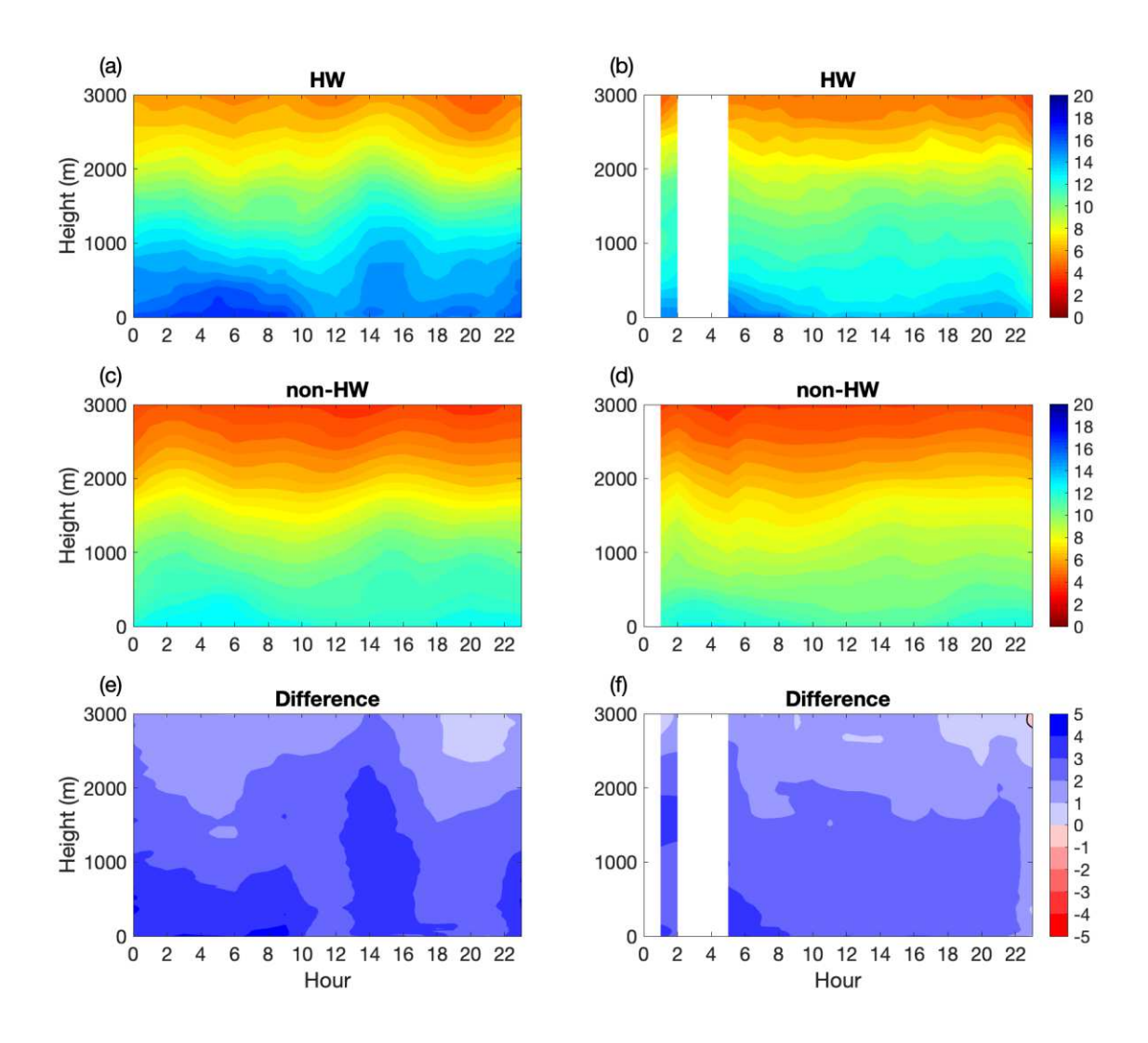


Figure 9. Diurnal variations of specific humidity during (a-b) HW and (c-d) non-HW periods in the lowest 3000 m above the ground averaged from 2007 to 2016, and (e-f) HW-related changes. The left column shows results at SDF and the right column shows results at PHL. Black lines in (e-f) indicate zero values. Units are g/kg.

A high evaporation demand during HW periods does not always lead to an increase in specific humidity, especially when the surface is dry (van Heerwaarden et al., 2010; Santanello et al., 2007). At DEN, the specific humidity at the surface and in the PBL is much lower than the other three airports, which can be seen in Figures 3m-p, 10 and 11. The relatively dry conditions are

associated with its location at a high elevation area adjacent to the Rocky Mountains, where the soil is typically dry (Findell and Eltahir, 2003; Santanello et al., 2018). The HW-related changes in specific humidity are generally negative in the PBL and the decreases of specific humidity during HW periods reduce with height (Figure 10f). For dry soils, in spite of high evaporation demand during HWs, surface evaporation is suppressed by the low supply of soil water, which in turn enhances the sensible heat flux (a positive feedback on the HW intensity). On this basis, entrainment brings drier air into the PBL as the convective PBL deepens (Santanello et al., 2007). This may be an important cause of the decreases in specific humidity at DEN. In addition, the HW events in this area are caused by persistent high-pressure systems, as shall be seen later. The downward motions or large-scale subsidence caused by such systems bring dry air loft into the lower troposphere, which can further cause humidity decreases in the lower troposphere. The humidity difference between HW and non-HW periods is also affected by the moisture transport. At HOU, the specific humidity decreases in the PBL while increases above the PBL under HWs compared to the non-HW periods (Figure 10e). This is because the HOU airport is located near the coast (Figure 1) and the moisture transport from the Gulf of Mexico is an important source of moisture at HOU. According to the differences in zonal and meridional winds between HW and non-HW periods at HOU shown in Figure 8e-f, the wind difference is positive for zonal wind but negative for meridional wind in the PBL, so the wind difference vector is from land to sea, which reduces the moisture transport and hence reduces the specific humidity over HOU. Conversely, the wind difference between HW and non-HW periods is negative for zonal wind above the PBL, which enhances the moisture transport from sea to land

384

385

386

387

388

389

390

391

392

393

394

395

396

397

398

399

400

401

402

403

404

405

although the meridional wind difference direction remains from land to sea (Figure 8e-f). These

changes in wind components and the associated moisture transport partly explain the HW-related changes in specific humidity at HOU.

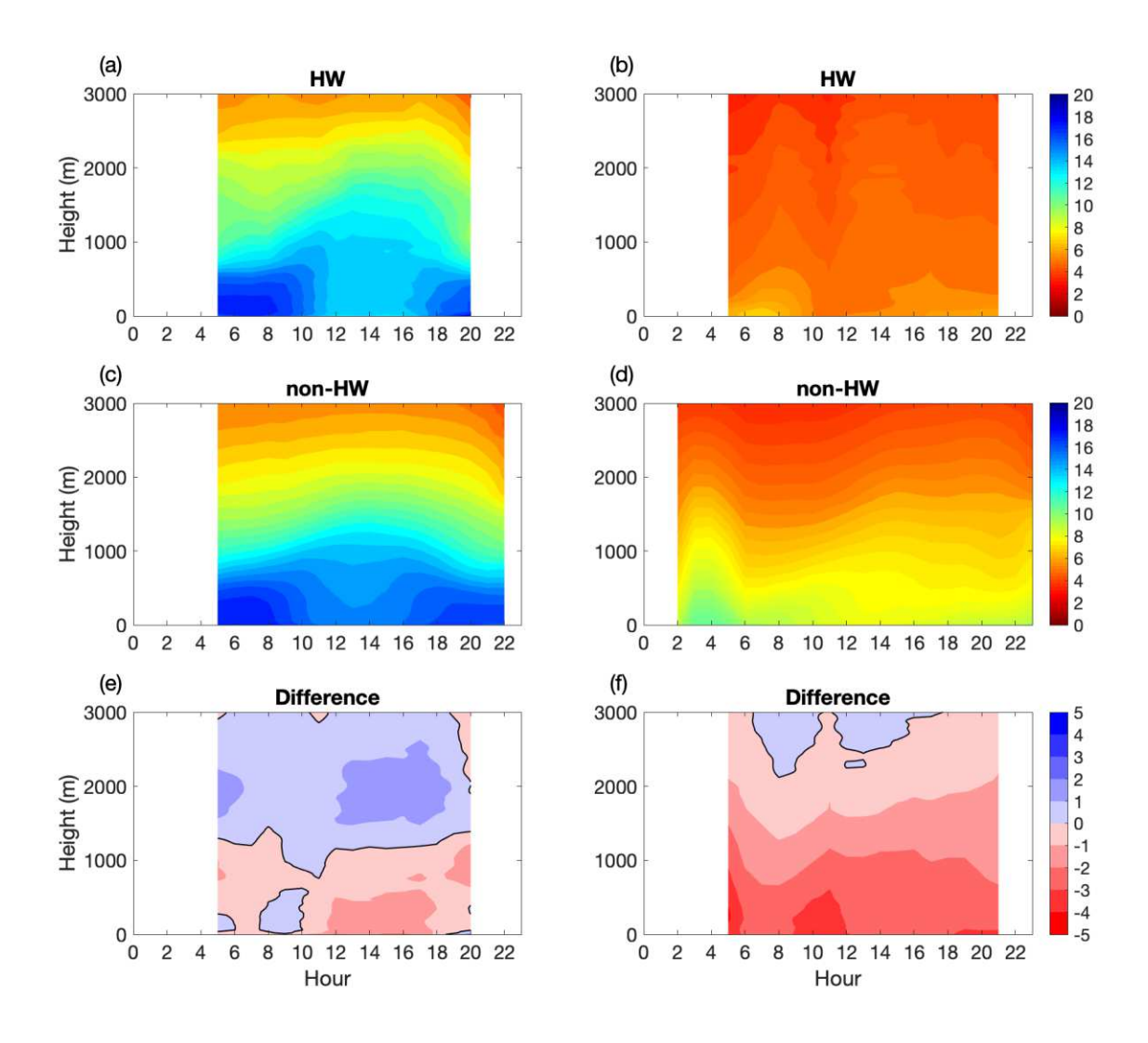


Figure 10. Similar to Figure 9, but at HOU (left) and DEN (right).

It should be noted that while the findings on HW-related changes in specific humidity are broadly consistent with previous studies on land-atmosphere feedbacks as discussed above and changes in wind components, the AMDAR data alone do not provide direct quantification of land-atmosphere feedbacks and advection terms. Further investigations using NARR data are conducted in Section 3.3 to verify these findings. It should be also pointed out that the AMDAR data might be affected by local factors such as urban land use and human activities (e.g., irrigation of lawns in suburban areas). The role of these local factors in modulating the PBL specific humidity under HWs needs to be further examined.

3.3 Impacts of synoptic-scale atmospheric circulation patterns and land-atmosphere

feedbacks on PBL wind and humidity during HWs

414

415

416

417

418

419

420

421

422

423

424

425

426

427

428

429

430

431

432

433

434

435

436

From the above case studies, it is clear that the characteristics of PBL during HW periods and the differences between HW and non-HW periods vary across climate regimes. To further investigate such spatial variability, Figure 11 shows the differences in PBL temperature, wind components, and specific humidity between HW and non-HW periods averaged from the surface to the PBL top in the AMDAR data (left) and those in the surface observations from weather stations (right). The PBL height is estimated by the bulk Richardson number method with a critical value of 0.25, as shown in Figure 6. The PBL and surface results in terms of temperature, zonal and meridional wind and specific humidity are broadly consistent, further confirming the reliability of AMDAR data. It can be seen that the PBL experiences warming under HW conditions across all airports (Figure 11a). This is expected given that HW is defined based on air temperature. For wind components, the differences of both zonal and meridional wind are mostly positive in the north and negative in the west. However, in the south, the differences are positive for zonal wind while mostly negative for meridional wind (Figure 11c and e). For specific humidity, the results indicate increases over most parts of the CONUS but decreases in the high elevation areas and south (Figure 11g). The largest increases in humidity are found in the central north and northeast with

values larger than 2 g/kg. Note that the differences in the PBL humidity at several airports are not shown because of data limitation.

To explain these spatial variations (especially those of wind and humidity), we investigate the atmospheric circulation patterns and surface evaporation associated with HWs in three different regions highlighted by the black circles in Figure 11c, e and g. These three regions are the northeastern region, Texas, and the high elevation region, which are referred as the Atlantic Seaboard, South, and Plateau regions hereinafter. Airports in the Atlantic Seaboard region include MHT, BOS, BDL, LGA, JFK, EWR, PHL, BWI, IAD, and DCA, while airports in the South region include DFW, BSM, SAT, IAH, and HOU. The airports DEN, ABQ, and SLC are within the Plateau region. We define regional HW periods as the sum of HW periods of all airports within the region.

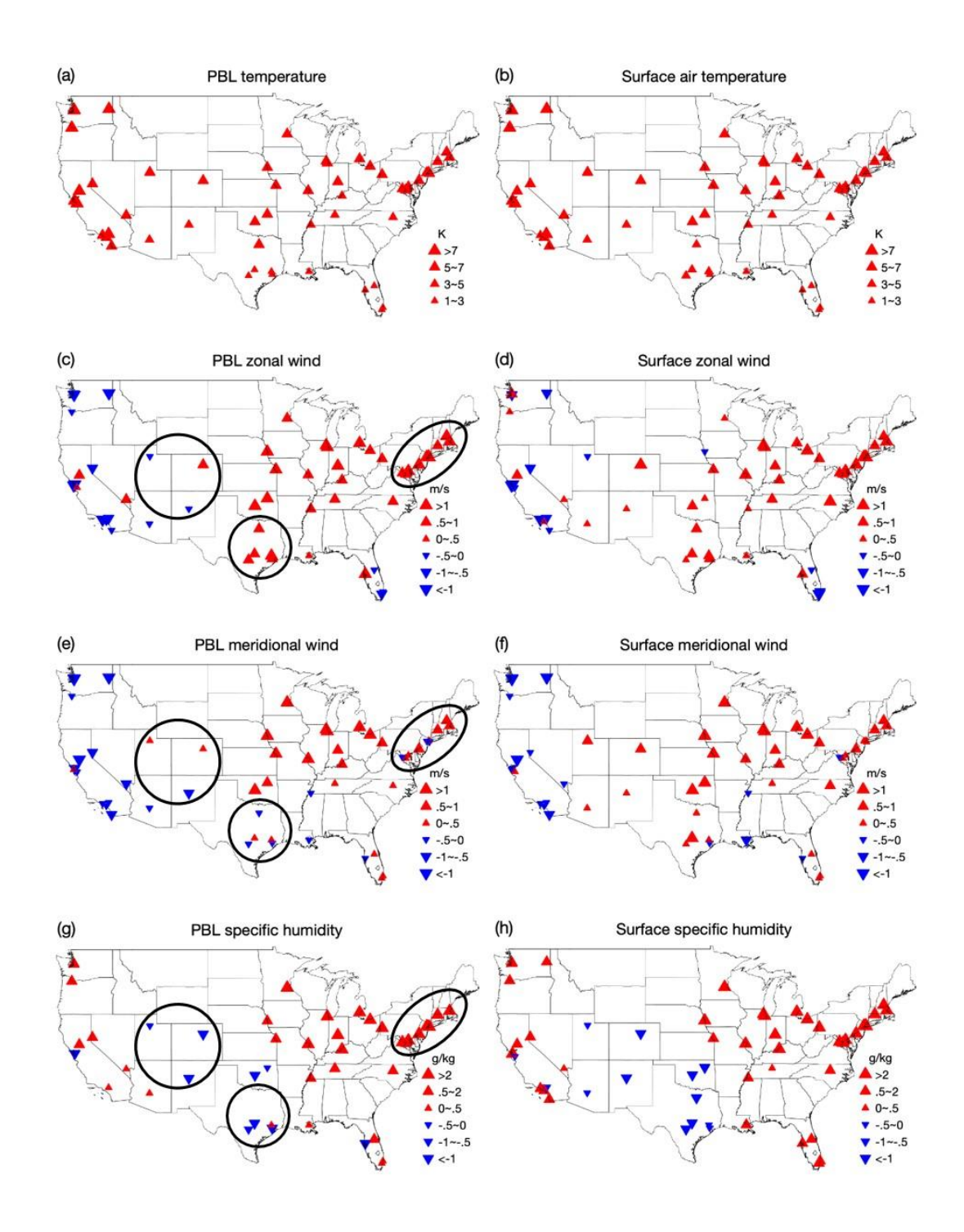


Figure 11. Differences in (a-b) temperature, (c-d) zonal wind, (e-f) meridional wind, and (g-h) specific humidity between HW and non-HW periods (HW minus non-HW) from AMDAR data under the PBL top (left) and surface observations (right) during 2007-2016. The black circles in (c, e, g) indicate the Atlantic Seaboard, South and Plateau regions, respectively, which are analyzed in Figure 12.

The geopotential height fields averaged over non-HW and HW periods and their differences for these three different regions are shown in Figure 12. HWs in the northeastern US are accompanied by the strengthening of the North Atlantic Subtropical High (NASH), which is a semi-permanent high-pressure system over the North Atlantic Ocean (Li et al., 2012). Following previous studies (Li et al., 2011), the 1,560 gpm isoline at 850 hPa is selected to represent the boundary of the NASH, shown as the black thick solid lines in Figure 12. It can be seen that compared to non-HW periods, the NASH is stronger and expands to the west and north during the regional HW periods for the Atlantic Seaboard region (c.f. Figure 12b to 12a) to form an anomalous high pressure (Figure 12c). The Atlantic Seaboard region is just located in the north of the anomalous high, where a wind vector anomaly from the west to the east is induced (see also in Figure S3b). This explains the increase of zonal wind during HW periods relative to non-HW periods in this region (Figure 11c). The northward movement of NASH also helps bring moisture from Northwest Atlantic and the Gulf of Mexico to the Atlantic Seaboard region, which contributes to the increase of specific humidity over the north and northeast (Figure 11g).

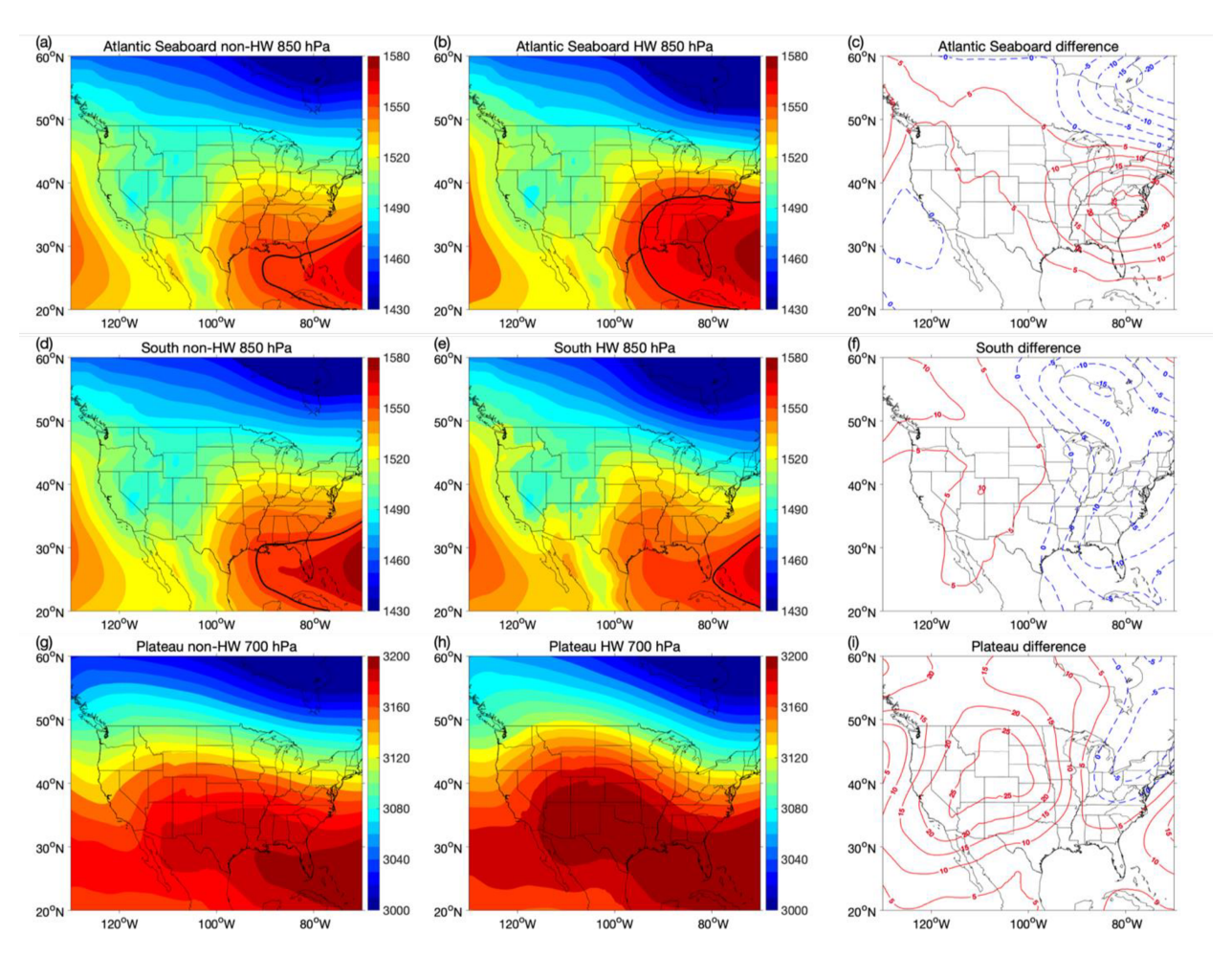


Figure 12. Geopotential height fields during non-HW (left), HW periods (middle) and their differences (right) in (a-c) the Atlantic Seaboard region at 850 hPa, (d-f) the South region at 850 hPa, and (g-i) the Plateau region at 700 hPa. The thick solid line in (a-b) and (d-e) is the 1,560 gpm contour line. Results have been averaged from 2007 to 2016 and units are m.

The South region is affected by low-level jets in summer, which bring moist air from the Gulf of Mexico to the southern and central US (Higgins et al., 1997). But during the regional HW periods for the South region, the NASH retreats eastward (c.f. Figure 12e to 14d), and anomalous high and low exist in the west and east of the South region, respectively (Figure 12f). This anomalous pressure pattern leads to a southward wind vector anomaly (see also in Figure S3e), which partly causes the reduction of the meridional wind in the South region (Figure 11e). However, changes in the geopotential height fields cannot explain the increase of the zonal wind

483 during HW periods in the South region. The southward wind vector anomaly also weakens the southwestern low-level jet and thus reduces moisture transport from the ocean to the land. This is 484 consistent with the decreases in the PBL specific humidity in the South region (Figure 11g). 485 The mean elevation of the three airports in the Plateau region is about 1500 m above the sea level. 486 As a result, the geopotential height fields at 700 hPa, which approximately corresponds to the 487 PBL height from the ground, are analyzed (Figure 12g-i). Compared to non-HW periods, there is 488 an anomalously high-pressure center over the Plateau region during HW periods (Figure 12i). 489 This anomalous high is usually a stationary system, which is often referred to as a blocking high 490 (e.g., Coughlan, 1983). The anomalous high leads to a wind vector from the northeast to the 491 492 southwest on its southern edge, which contributes to decreases of the zonal and meridional wind at ABQ (the southernmost airport within the Plateau region, Figure 11c and e). The other two 493 airports in the Plateau region (SLC and DEN) are located at the center of the anomalous high. 494 495 Hence their changes in wind components are less affected by changes in the geopotential height field but may be more associated with changes in secondary-circulations. 496 Figure 13 shows the differences of surface latent heat fluxes averaged over non-HW and HW 497 498 periods for these three regions. In the Atlantic Seaboard region, surface evaporation is enhanced 499 during HW periods (Figure 13a), which contributes to the increases of specific humidity over 500 this region as discussed in Section 3.2.3 (see also Figure 11g). In the South region, surface latent heat flux decreases during HW periods (Figure 13b). This is largely because surface evaporation 501 502 is suppressed by the lack of soil water during HW periods. This contributes to the decreases of the specific humidity over this region under HWs (see Figure 11g). In the Plateau region, surface 503 latent heat flux has no significant HW-related changes (Figure 13c), which is because surface 504 evaporation is small during both HW and non-HW periods due to dry soil. The decrease of 505

specific humidity in the PBL (Figure 11g) is possibly a result of the positive land-atmosphere feedbacks under dry conditions as already discussed in Section 3.2 (Santanello et al., 2007). That is, the sensible heat flux and the PBL height increase (see Figure 6). In this process, the PBL specific humidity decreases as dry air is brought into the PBL by entrainment and the downward motion caused by the blocking high.

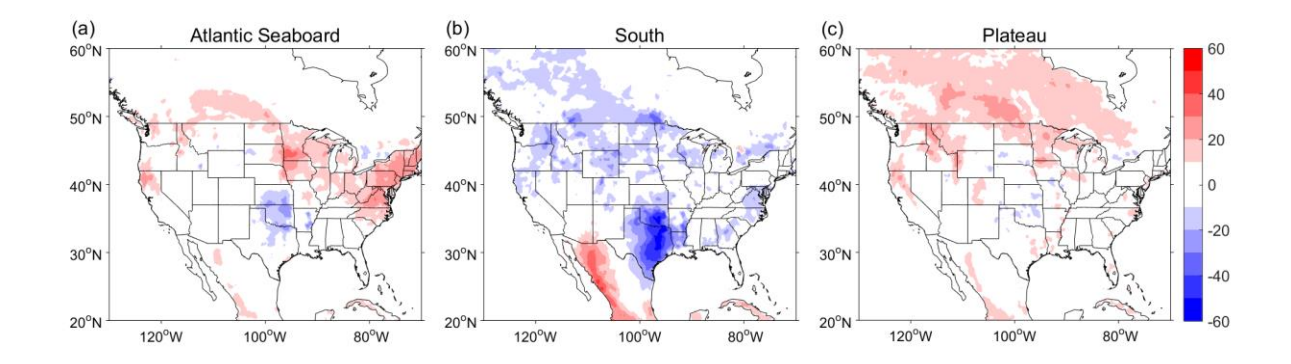


Figure 13. Differences in surface latent heat flux (W/m²) from NARR daily data between HW and non-HW periods (HW minus non-HW) in (a) the Atlantic Seaboard region, (b) the South region, and (c) the Plateau region during 2007-2016.

In summary, the HWs over the Atlantic Seaboard, South and Plateau regions are associated with the northward movement and strengthening of the NASH, the weakening of the southwestern LLJ and an anomalous high, respectively. These synoptic-scale circulation patterns have important implications for HW-related changes in the PBL. In addition, land-atmosphere feedbacks are expected to play an important role in controlling HW-related changes in the PBL, especially specific humidity. Table 2 summarizes the observed changes in PBL quantities and the possible causes. It can be seen that while many observed changes can be explained by the

synoptic-scale circulation patterns and land-atmosphere feedbacks, the causes of some changes, such as increases of the meridional wind over the Atlantic Seaboard region and zonal wind over the South region, need to be further studied.

Table 2. HW-related changes in the PBL and the possible causes over Atlantic Seaboard, South and Plateau regions.

Variable	Region	HW-related changes	Possible causes				
Temperature	All regions	Increase	HW definition is based on air temperature				
	Atlantic Seaboard	Increase	Synoptic wind vector anomaly				
Zonal wind	South	Increase	Unclear				
	Plateau	Not uniform	Synoptic wind vector anomaly				
	Atlantic Seaboard	Mostly increase	Unclear				
Meridional wind	South Mostly de		Synoptic wind vector anomaly				
	Plateau	Not uniform	Synoptic wind vector anomaly				
	Atlantic Seaboard	Increase	Strengthened moisture transport and higher surface evaporation				
Specific humidity	c humidity South Mostly do		Weakened moisture transport and reduced surface evaporation				
	Plateau	Decreases	Dry air subsidence and entrainment				

4. Conclusions

This study investigates the diurnal variations of the PBL characteristics under HWs at 54 major airports across CONUS based on a decade-long (from 2007 to 2016) data record of hourly profiles from commercial aircrafts (the AMDAR data). The HW periods at each airport are identified based on surface air temperature observations and defined as at least 2 consecutive days with daily mean temperature exceeding the 95th percentile of the warm season (May to September) climatology. The mean differences in the surface and PBL temperature, wind

components, and specific humidity between HW and non-HW periods are analyzed. The AMDAR profiles have been extensively validated against collocated radiosonde data in our recent study (Zhang et al., 2019) but the consistency between the results using surface observations and AMDAR data averaged over 20-100 m provides further confidence to the quality of the AMDAR data.

Under HWs, heat domes are observed. During the daytime, the strong HW-related warming

occurs throughout the PBL with the maximum near the surface, which contributes to the development of the convective PBL. At night, the strong HW-related warming above the PBL top is in favor of the formulation of deep and warm nocturnal residual layers. The heat stored in the nocturnal residual layer further contributes to the PBL warming in the following day.

There are clear vertical and diurnal variations in the PBL wind and humidity changes, which are also spatially non-uniform. Most (but not all) of the HW-related changes in wind components can be explained by changes in synoptic-scale atmospheric circulation patterns. In the northeastern US, HWs are usually accompanied by an anomalous high due to the enhancement and northward extension of NASH, which contributes to the increases in zonal wind. In Texas, the anomalous pressure field during HWs leads to a southward wind vector, which reduces the meridional wind.

The HW-related changes in the PBL specific humidity are associated with surface evaporation moisture transport, and dry air entrainment. In the northeast, the increases in PBL specific humidity are associated with enhanced moisture transport and surface evaporation under HWs. In contrary, the weakened moisture transport and surface evaporation contribute to the decreases in PBL specific humidity in Taxes during HWs. In the high elevation region, the specific humidity decreases likely due to the combined effects of land-atmosphere feedbacks, the large-

scale subsidence under high pressure conditions, and dry air entrainment along with the PBL growth.

This study presents an important application of AMDAR data in meteorology and climatology, namely, examining the diurnal variations of PBL during HWs. While this study improves our scientific understanding of HW-related changes in the PBL structure and highlights their possible connections with the synoptic-scale atmospheric circulation patterns and land-atmosphere feedbacks, future research examining the role of PBL in the onset and demise of HWs and examining whether meteorological models can capture the observed response of the PBL to HWs is strongly needed.

Acknowledgments

YZ, ZP, and ZG acknowledge support from the National Natural Science Foundation of China (Grants No. 41705004 and No. 41275022), the Natural Science Foundation of Jiangsu Province (Grants No. SBK2017041444). YZ is also supported by the Talent Start-up Foundation of Nanjing University of Information Science and Technology (Grants No. 2016r056) and the scholarship under the State Scholarship Fund (No. 201708320030). LW and DL acknowledge supported from the U.S. Army Research Office under Grant No. W911NF-18-1-0360 and the U.S. National Science Foundation under Grant No. 1854706. This work was conducted when the first author visited Boston University in 2017-2018. The AMDAR data are available on the Meteorological Assimilation Data Ingest System web service portal (https://madisdata.cprk.ncep.noaa.gov/madisPublic1/data/archive/). The processed profiles can be obtained from the corresponding author upon request.

References

- Ackerman, S., Knox, J.A., 2006. Meteorology: understanding the atmosphere. Cengage Learning.
- Alexander, L., 2011. Extreme heat rooted in dry soils. Nat. Geosci. 4, 12–13.
- 585 https://doi.org/10.1038/ngeo1045.
- Anderson, B.G., Bell, M.L., 2009. Weather-related mortality: how heat, cold, and heat waves
- affect mortality in the United States. Epidemiology (Cambridge, Mass.) 20, 205.
- Anderson, G.B., Bell, M.L., 2011. Heat waves in the United States: mortality risk during heat
- waves and effect modification by heat wave characteristics in 43 US communities.
- Environ. Health Perspect. 119, 210-218.
- Ao, X., Wang, L., Zhi, X., Gu, W., Yang, H., Li, D., 2019. Observed synergies between urban
- heat islands and heat waves and their controlling factors in Shanghai, China. J. Appl.
- 593 Meteorol. Clim. 2019.
- Ballish, B.A., Kumar, V.K., 2008. Systematic Differences in Aircraft and Radiosonde
- Temperatures: Implications for NWP and Climate Studies. Bull. Am. Meteorol. Soci.
- 596 89(11), 1689–1708. https://doi.org/10.1175/2008BAMS2332.1
- Barnett, A.G., Tong, S., Clements, A.C.A., 2010. What measure of temperature is the best
- 598 predictor of mortality? Environ. Res. 110, 604–611.
- 599 https://doi.org/10.1016/j.envres.2010.05.006.
- Benjamin, S.G., Schwartz, B.E., Cole, R.E., 1999. Accuracy of ACARS Wind and Temperature
- Observations Determined by Collocation. Weather Forecast. 14, 1032–1038.
- Bisiaux, M., Cox, M.E., Forrester, D.A., Storey, J.T., 1983. Possible improvements in
- meteorology for aircraft navigation. J. Navigation 36, 54-63.

- Black, E., Blackburn, M., Harrison, G., Hoskins, B., Methven, J., 2004. Factors contributing to
- the summer 2003 European heatwave. Weather 59, 217–223.
- 606 Cassou, C., Terray, L., Phillips, A.S., 2005. Tropical Atlantic Influence on European Heat Waves.
- J. Clim. 18, 2805–2811. https://doi.org/10.1175/JCLI3506.1.
- 608 Coughlan, M., 1983. A comparative climatology of blocking action in the two hemispheres. Aust.
- 609 Meteorol. Mag. 31, 3–13.
- 610 Coumou, D., Rahmstorf, S., 2012. A decade of weather extremes. Nat. Clim. Change 2, 491.
- De Boeck, H.J., Dreesen, F.E., Janssens, I.A., Nijs, I., 2010. Climatic characteristics of heat
- waves and their simulation in plant experiments: HEAT WAVE CHARACTERISTICS
- AND SIMULATION. Global Change Biol. 16, 1992–2000.
- 614 https://doi.org/10.1111/j.1365-2486.2009.02049.x.
- Durre, I., Wallace, J.M., Lettenmaier, D.P., 2000. Dependence of Extreme Daily Maximum
- Temperatures on Antecedent Soil Moisture in the Contiguous United States during
- 617 Summer. J. Clim. 13, 2641–2651.
- Epstein, Y., Moran, D.S., 2006. Thermal comfort and the heat stress indices. Ind. Health 44,
- 619 388–398.
- 620 Findell, K.L., Eltahir, E.A.B., 2003. Atmospheric controls on soil moisture–boundary layer
- interactions: Part II: Feedbacks within the continental United States. J. Hydrometeor. 4,
- 622 570–583.
- Fischer, E.M., Seneviratne, S.I., Lüthi, D., Schär, C., 2007a. Contribution of land-atmosphere
- coupling to recent European summer heat waves. Geophys. Res. Lett. 34.
- https://doi.org/10.1029/2006GL029068.

- Fischer, E.M., Seneviratne, S.I., Vidale, P.L., Lüthi, D., Schär, C., 2007b. Soil Moisture–
- Atmosphere Interactions during the 2003 European Summer Heat Wave. J. Clim. 20,
- 628 5081–5099. https://doi.org/10.1175/JCLI4288.1
- 629 Frich, P., Alexander, L.V., Della-Marta, P.M., Gleason, B., Haylock, M., Tank, A.K., Peterson,
- T., 2002. Observed coherent changes in climatic extremes during the second half of the
- twentieth century. Clim. Res. 19, 193–212.
- Hidalgo, J., Masson, V., Gimeno, L., 2010: Scaling the daytime urban heat island and urban-
- breeze circulation. J. Appl. Meteor. Climatol., 49, 889–901.
- Higgins, R.W., Yao, Y., Yarosh, E.S., Janowiak, J.E., Mo, K.C., 1997. Influence of the Great
- Plains low-level jet on summertime precipitation and moisture transport over the central
- 636 United States. J. Clim. 10, 481–507.
- Hong, S.Y., 2010. A new stable boundary-layer mixing scheme and its impact on the simulated
- East Asian summer monsoon. Q. J. R. Meteorol. Soc. 136, 1481–1496.
- Karl, T.R., Knight, R.W., 1997. The 1995 Chicago heat wave: How likely is a recurrence? Bull.
- 640 Am. Meteorol. Soc. 78, 1107–1120.
- Lau, N.C., Nath, M.J., 2012. A model study of heat waves over North America: Meteorological
- aspects and projections for the twenty-first century. J. Clim. 25, 4761–4784.
- Lau, N.C., Nath, M.J., 2014. Model simulation and projection of European heat waves in
- present-day and future climates. J. Clim. 27, 3713–3730.
- Lebassi, B., González, J., Bornstein, R., 2011. Modeled large-scale warming impacts on summer
- 646 California coastal-cooling trends. J. Geophys. Res.: Atmos. 116(D20).

- Lebassi, B., González, J., Fabris, D., Maurer, E., Miller, N., Milesi, C., Switzer, P., Bornstein, R.,
- 648 2009. Observed 1970–2005 cooling of summer daytime temperatures in coastal
- 649 California. J. Clim. 22, 3558–3573.
- 650 Li, D., Bou-Zeid, E., 2013. Synergistic interactions between urban heat islands and heat waves:
- The impact in cities is larger than the sum of its parts. J. Appl. Meteorol. Clim. 52, 2051–
- 652 2064.
- Li, D., Sun, T., Liu, M., Wang, L., Gao, Z., 2016. Changes in Wind Speed under Heat Waves
- Enhance Urban Heat Islands in the Beijing Metropolitan Area. J. Appl. Meteorol. Clim.
- 55, 2369–2375. https://doi.org/10.1175/JAMC-D-16-0102.1.
- 656 Li, D., Sun, T., Liu, M., Yang, L., Wang, L., Gao, Z., 2015. Contrasting responses of urban and
- rural surface energy budgets to heat waves explain synergies between urban heat islands
- and heat waves. Environ. Res. Lett. 10(5), 054009.
- 659 Li, L., Li, W., Kushnir, Y., 2012. Variation of the North Atlantic subtropical high western ridge
- and its implication to Southeastern US summer precipitation. Clim. Dynam. 39, 1401–
- 661 1412. https://doi.org/10.1007/s00382-011-1214-y.
- 662 Li, W., Li, L., Fu, R., Deng, Y., Wang, H., 2011. Changes to the North Atlantic Subtropical High
- and Its Role in the Intensification of Summer Rainfall Variability in the Southeastern
- United States. J. Clim. 24, 1499–1506. https://doi.org/10.1175/2010JCLI3829.1.
- 665 Li, W., Zou, T., Li, L., Deng, Y., Sun, V.T., Zhang, Q., Layton, J.B., Setoguchi, S., 2019.
- Impacts of the North Atlantic subtropical high on interannual variation of summertime
- heat stress over the conterminous United States. Clim. Dynam. 1-15.
- https://doi.org/10.1007/s00382-019-04708-1.

- 669 Liao, W., Liu, X., Li, D., Luo, M., Wang, D., Wang, S., Baldwin, J., Lin, L., Li, X., Feng, K.,
- Hubacek, K., Yang, X., 2018. Stronger Contributions of Urbanization to Heat Wave
- Trends in Wet Climates. Geophys. Res. Lett. 45. https://doi.org/10.1029/2018GL079679.
- Liu, Y., Pan, Z., Zhuang, Q., Miralles, D.G., Teuling, A.J., Zhang, T., An, P., Dong, Z., Zhang, J.,
- He, D., Wang, L., Pan, X., Bai, W., Niyogi, D., 2015. Agriculture intensifies soil
- moisture decline in Northern China. Sci. Rep. 5, 11261.
- https://doi.org/10.1038/srep11261.
- Lorenz, R., Jaeger, E.B., Seneviratne, S.I., 2010. Persistence of heat waves and its link to soil
- 677 moisture memory. Geophys. Res. Lett. 37. https://doi.org/10.1029/2010GL042764.
- Matzarakis, A., Nastos, P.T., 2011. Human-biometeorological assessment of heat waves in
- Athens. Theor. Appl. Clim. 105, 99–106. https://doi.org/10.1007/s00704-010-0379-3.
- McMichael, A.J., Lindgren, E., 2011. Climate change: present and future risks to health, and
- necessary responses. J. Intern. Med. 270, 401–413.
- Meehl, G.A., Tebaldi, C., 2004. More Intense, More Frequent, and Longer Lasting Heat Waves
- in the 21st Century. Science 305, 994–997. https://doi.org/10.1126/science.1098704.
- Meehl, G.A., Covey, C., Delworth, T., Latif, M., McAvaney, B., Mitchell, J.F., Stouffer, R.J.,
- Taylor, K.E., 2007. The WCRP CMIP3 multimodel dataset: A new era in climate change
- 686 research. Bull. Am. Meteorol. Soc. 88, 1383–1394.
- Miralles, D.G., van den Berg, M.J., Teuling, A.J., de Jeu, R.A.M., 2012. Soil moisture-
- temperature coupling: A multiscale observational analysis. Geophys. Res. Lett. 39.
- https://doi.org/10.1029/2012GL053703.

690 Miralles, D.G., Teuling, A.J., van Heerwaarden, C.C., Vilà-Guerau de Arellano, J., 2014. Megaheatwave temperatures due to combined soil desiccation and atmospheric heat 691 accumulation. Nat. Geo. 7, 345–349. https://doi.org/10.1038/ngeo2141. 692 Miralles, D.G., Gentine, P., Seneviratne, S.I., Teuling, A.J., 2018. Land-atmospheric feedbacks 693 during droughts and heatwaves: state of the science and current challenges: Land 694 feedbacks during droughts and heatwaves. Ann. N. Y. Acad. Sci. 695 https://doi.org/10.1111/nyas.13912. 696 Nasrallah, H.A., Nieplova, E., Ramadan, E., 2004. Warm season extreme temperature events in 697 698 Kuwait. J. Arid Environ. 56, 357–371. Ohashi, Y., Kida, H., 2002: Local circulations developed in the vicinity of both coastal and 699 inland urban areas: A numerical study with a mesoscale atmospheric model. J. Appl. 700 Meteor., 41, 30–45. 701 Perkins, S.E., 2015. A review on the scientific understanding of heatwaves—Their measurement, 702 driving mechanisms, and changes at the global scale. Atmos. Res. 164, 242–267. 703 https://doi.org/10.1016/j.atmosres.2015.05.014. 704 Petersen, R.A., 2016. On the impact and benefits of AMDAR observations in operational 705 706 forecasting—Part I: A review of the impact of automated aircraft wind and temperature reports. Bull. Am. Meteorol. Soci. 97, 585–602. 707 Petersen, R.A., Cronce, L., Mamrosh, R., Baker, R., Pauley, P., 2016. On the Impact and Future 708 709 Benefits of AMDAR Observations in Operational Forecasting: Part II: Water Vapor Observations. Bull. Am. Meteorol. Soci. 97, 2117–2133. https://doi.org/10.1175/BAMS-710

711

D-14-00211.1.

- Peterson, T.C., Heim, R.R., Hirsch, R., et al., 2013. Monitoring and Understanding Changes in
- Heat Waves, Cold Waves, Floods, and Droughts in the United States: State of Knowledge.
- Bull. Am. Meteorol. Soci. 94, 821–834. https://doi.org/10.1175/BAMS-D-12-00066.1.
- Radinović, D., Ćurić, M., 2012. Criteria for heat and cold wave duration indexes. Theor. Appl.
- 716 Clim. 107, 505–510.
- Ramamurthy, P., González, J., Ortiz, L., Arend, M., Moshary, F., 2017. Impact of heatwave on a
- megacity: an observational analysis of New York City during July 2016. Environ. Res.
- 719 Lett. 12, 054011.
- Robinson, P.J., 2001. On the Definition of a Heat Wave. J. Appl. Meteorol. 40, 762–775.
- 721 https://doi.org/10.1175/1520-0450(2001)040<0762:OTDOAH>2.0.CO;2.
- Santanello, J.A., Friedl, M.A., Ek, M.B., 2007. Convective Planetary Boundary Layer
- Interactions with the Land Surface at Diurnal Time Scales: Diagnostics and Feedbacks. J.
- Hydrometeorol. 8, 1082–1097. https://doi.org/10.1175/JHM614.1.
- Santanello, J.A., Dirmeyer, P.A., Ferguson, C.R., et al., 2018. Land–Atmosphere Interactions:
- The LoCo Perspective. Bull. Am. Meteorol. Soci. 99, 1253–1272.
- 727 https://doi.org/10.1175/BAMS-D-17-0001.1.
- Seneviratne, S.I., Corti, T., Davin, E.L., Hirschi, M., Jaeger, E.B., Lehner, I., Orlowsky, B.,
- 729 Teuling, A.J., 2010. Investigating soil moisture–climate interactions in a changing
- 730 climate: A review. Earth-Sci. Rev. 99, 125–161.
- 731 https://doi.org/10.1016/j.earscirev.2010.02.004.
- 732 Smith, T.T., Zaitchik, B.F., Gohlke, J.M., 2013. Heat waves in the United States: definitions,
- patterns and trends. Clim. Change 118, 811–825. https://doi.org/10.1007/s10584-012-
- 734 0659-2.

- 735 Sun, T., Kotthaus, S., Li, D., Ward, H.C., Gao, Z., Ni, G.H., Grimmond, C.S.B., 2017.
- Attribution and mitigation of heat wave-induced urban heat storage change. Environ. Res.
- 737 Lett. 12, 114007.
- 738 Teuling, A.J., Seneviratne, S.I., Stöckli, R., et al., 2010. Contrasting response of European forest
- and grassland energy exchange to heatwaves. Nat. Geo. 3, 722–727.
- 740 https://doi.org/10.1038/ngeo950.
- 741 Teuling, A.J., Van Loon, A.F., Seneviratne, S.I., Lehner, I., Aubinet, M., Heinesch, B.,
- Bernhofer, C., Grünwald, T., Prasse, H., Spank, U., 2013. Evapotranspiration amplifies
- European summer drought. Geophys. Res. Lett. 40, 2071–2075.
- van Heerwaarden, C.C., Vilà-Guerau de Arellano, J., Gounou, A., Guichard, F., Couvreux, F.,
- 745 2010. Understanding the Daily Cycle of Evapotranspiration: A Method to Quantify the
- Influence of Forcings and Feedbacks. J. Hydrometeorol. 11, 1405–1422.
- 747 https://doi.org/10.1175/2010JHM1272.1.
- Vautard, R., Gobiet, A., Jacob, D., et al., 2013. The simulation of European heat waves from an
- ensemble of regional climate models within the EURO-CORDEX project. Clim. Dynam.
- 750 41, 2555–2575. https://doi.org/10.1007/s00382-013-1714-z.
- Vogelezang, D.H.P., Holtslag, A.A.M., 1996. Evaluation and model impacts of alternative
- boundary-layer height formulations. Bound.-Lay. Meteorol. 81, 245–269.
- Weisheimer, A., Palmer, T.N., 2014. On the reliability of seasonal climate forecasts. J. R. Soc.
- 754 Interface 11, 20131162. https://doi.org/10.1098/rsif.2013.1162.
- 755 Xoplaki, E., Gonzalez-Rouco, J.F., Luterbacher, J., Wanner, H., 2003. Mediterranean summer air
- 756 temperature variability and its connection to the large-scale atmospheric circulation and
- 757 SSTs. Clim. Dynam. 20, 723–739.

Zhang, K., Li, Y., Schwartz, J.D., O'Neill, M.S., 2014a. What weather variables are important in 758 predicting heat-related mortality? A new application of statistical learning methods. 759 Environ. Res. 132, 350–359. https://doi.org/10.1016/j.envres.2014.04.004. 760 761 Zhang, Y., Gao, Z., Li, D., Li, Y., Zhang, N., Zhao, X., Chen, J., 2014b. On the computation of planetary boundary-layer height using the bulk Richardson number method. Geosci. 762 Model Dev. 7, 2599-2611. 763 Zhang, Y., Li, D., Lin, Z., Santanello, J.A., Gao, Z., 2019. Development and evaluation of a 764 long-term data record of planetary boundary layer profiles from aircraft meteorological 765 reports. J. Geophys. Res.: Atmos. 124. https://doi.org/10.1029/2018JD029529. 766 Zuo, J., Pullen, S., Palmer, J., Bennetts, H., Chileshe, N., Ma, T., 2015. Impacts of heat waves 767 and corresponding measures: a review. J. Clean. Prod. 92, 1–12. 768

https://doi.org/10.1016/j.jclepro.2014.12.078.